Open access • Report • DOI:10.2172/1468158

Development of Preliminary VERA-CS Crud Induced Localized Corrosion Modeling Capability — Source link 🔗

Robert Salko, Stuart R. Slattery, Travis Lange, Marc-Oliver Delchini ...+3 more authors

Institutions: Oak Ridge National Laboratory, University of Texas at Austin, Westinghouse Electric

Published on: 01 Jun 2018

Topics: Corrosion

Development of Preliminary VERA-CS Crud-Induced Localized Corrosion Modeling Capability
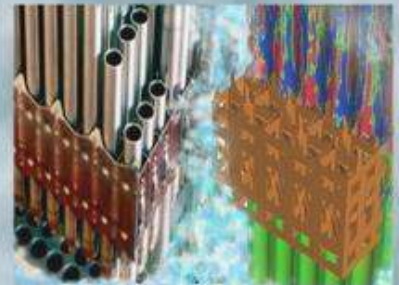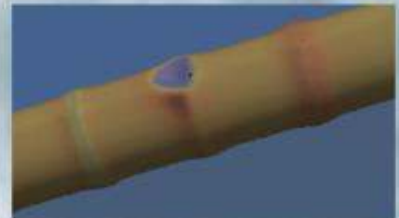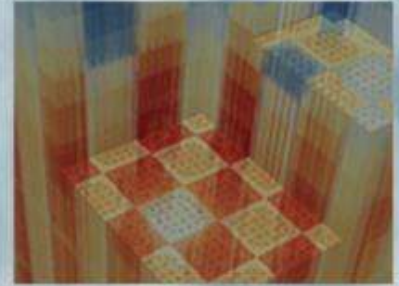
Milestone: L2:PHI.P17.03

Robert Salko[1], Stuart Slattery[1], Travis Lange[1], Marc-Oliver Delchini[1], William Gurecky[2], Emre Tatli[3], and Benjamin Collins[1]

[1]Oak Ridge National Laboratory
[2]University of Texas, Austin
[3]Westinghouse Electric Company

6/15/2018

U.S. DEPARTMENT OF ENERGY | Nuclear Energy

Revision Log

Revision	Date	Affected Pages	Revision Description
0	6/15/2018	All	Initial Release

Document pages that are:

Export Controlled:	None
IP/Proprietary/NDA Controlled:	None
Sensitive Controlled:	None
Unlimited:	All

Requested distribution:

To:

Kevin Clarno, David Kropacek, Richard Martineau

Copy: Jeff Banta

EXECUTIVE SUMMARY

The objective of this milestone was to develop a crud-induced localized corrosion (CILC) screening capability in VERA-CS using existing codes and capabilities that had been developed in the Consortium for Advanced Simulation of Light Water Reactors (CASL) as part of the efforts to resolve the crud challenge problem. The milestone work focused on improving existing CASL software and implementing clad corrosion modeling into VERA-CS. Clad corrosion modeling was implemented by creating an application interface (API) in the Cicada software so that its clad heat transfer and corrosion models could be used in VERA-CS. Cicada was coupled to the subchannel code CTF for solving crud and corrosion growth. Additionally, a clad corrosion model was added directly to CTF to serve as an alternate approach. The rod thermal hydraulic reconstruction (ROTHCON) process, which is used for capturing computational fluid dynamics (CFD)-predicted rod-surface heat and turbulence behavior that can impact crud-induced power shift (CIPS) and CILC prediction, was also implemented into VERA-CS. Usability improvements were made to this feature, which was developed over several previous milestones, so that the VERA-CS user can link spacer grids in a VERA-CS model to an applicable pregenerated spacer grid data file if available.

Several assessments were performed to demonstrate the proper functioning of the new capability. Sensitivity studies were performed to demonstrate the effect of crud lithium content, oxide thermal conductivity, Cicada mesh refinement, and ROTHCON coupling mesh refinement on predicted amounts of crud and oxide growth. A full-scale demonstration was performed by running Seabrook Cycle 5 with the CILC capability.

Some general observations were made from the assessments. It was observed that predicted corrosion thickness is less than anticipated for CILC cases, so further work is needed to better understand and improve the corrosion modeling. Refining the coupling mesh in the ROTHCON process leads to increased corrosion and crud thickness, which can affect where crud and corrosion grow, how thick it gets, and how many rods experience crud and corrosion growth. Results indicate that applying the ROTHCON process and refining the coupling mesh leads to only a slight increase in total core maximum crud and corrosion thickness, but it leads to a significant increase in the number of rods with a maximum thickness that surpasses a set threshold value (i.e., more rods grow thicker corrosion and crud). Computational performance of the simulation is degraded by a factor of 5–6 with high coupling mesh refinement. The impact of the ROTHCON coupling mesh refinement on total core crud mass is less significant; however, using the ROTHCON process with CFD-generated data over the Yao–Hochreiter–Leech (YHL) model in CTF leads to significantly different amounts of total core crud mass. Future work on the CILC screening capability will include model improvement and validation, development and testing of a CILC-risk screening criteria, and performance improvements.

(This page intentionally left blank)

CONTENTS

(This page intentionally left blank)

FIGURES

TABLES

ACRONYMS

1D one-dimensional

2D two-dimensional

3D three-dimensional

AMA Advanced Modeling Applications

API application interface

CAD computer-aided drafting

CASL Consortium for Advanced Simulation of Light Water Reactors

CILC crud-induced localized corrosion

CFD computational fluid dynamics

CIPS crud-induced power shift

DNB departure from nucleate boiling

EFPD effective full power days

HTC heat transfer coefficient

IFBA integral fuel burnable absorber

LWR light water reactor

ORNL Oak Ridge National Laboratory

PWR pressurized water reactor

RMSE root-mean-square error

ROTHCON rod thermal hydraulic reconstruction

T/H thermal-hydraulics

TKE turbulent kinetic energy

VERAIn VERA-CS common input file

WEC Westinghouse Electric Company

YHL Yao–Hochreiter–Leech

(This page intentionally left blank)

1 INTRODUCTION

Crud-induced localized corrosion falls under the broader category of the crud challenge problem, which is one of the six major issues being studied and addressed by Consortium for Advanced Simulation of Light Water Reactors (CASL). The crud challenge problem includes crud-induced power shift (CIPS) and crud-induced localized corrosion (CILC), both of which result from circulating particulate and soluble coolant corrosion products depositing on fuel rod surfaces. During normal light water reactor (LWR) operation, an oxide layer grows on the exterior of the fuel rod cladding due to interaction with the primary side coolant [1]. Formation of crud deposits can accelerate the growth of this oxide layer due to the crud chemical composition and its thermal resistance and impact on clad surface temperature [2]. CILC is encountered in LWRs and is limiting because it can lead to fuel rod failures as the cladding thins. Prediction of this phenomenon requires the ability to predict core chemistry and coolant corrosion product content, crud deposition, crud chemistry, and local thermal-hydraulic and neutronic behavior.

This work builds on previous milestones to realize a preliminary capability for performing CILC-risk screening in LWRs. Past work has led to the development and improvement of a clad chemistry code, MAMBA, which is used to predict growth and erosion of crud deposits on fuel rod surfaces as a function of local chemistry and thermal-hydraulics (T/H) conditions [3]. This capability has been coupled to the T/H subchannel code CTF and the neutron transport code MPACT in VERA-CS [4].

Work has also been done to couple MAMBA to the commercial computational fluid dynamics (CFD) code STAR-CCM+ for more highly resolved modeling of crud behavior [5, 6]. This work has led to the development of the Cicada code, which (1) provides an interface to STAR-CCM+ for driving coupled crud and T/H simulations and (2) provides a 3D solver for clad corrosion and T/H. Part of this milestone focused on developing an application interface (API) for Cicada and coupling it to VERA-CS.

Previous studies found that the resolution of rod surface T/H behavior can be important for properly modeling crud growth and effects [7]. This led to the development of a process in which high-fidelity CFD T/H data can be reconstructed onto the rod surface in the lower-fidelity subchannel code [8]. This process is herein referred to as the rod thermal hydraulic reconstruction (ROTHCON) process. Rod surface heat transfer and near-wall turbulent kinetic energy (TKE) are the two T/H data of interest that are included in the reconstruction. This milestone provided for usability improvements to this feature so it can be used in a VERA-CS simulation. It also allowed for the conduct of sensitivity studies to determine its effect on crud and corrosion growth.

The goal of this milestone is to build on the existing work to develop a CILC screening capability in VERA-CS that can be delivered to the Advanced Modeling Applications (AMA) focus area for performing full-core-scale CILC assessments. The intention is for AMA to use the tool developed in this milestone to begin identifying areas in the core that are at risk of experiencing CILC using metrics such as predicted crud and corrosion thickness. Features and models needed for CILC modeling have been implemented, with an emphasis on delivering a product that has a high degree of usability and that provides input and output options required to perform a rigorous analysis. The following path was taken to complete this milestone.

1. Create an API in the Cicada code to use in solving clad/oxide temperature and oxide growth

2. Couple Cicada to VERA-CS

3. Implement a clad exterior corrosion model in CTF

4. Incorporate usability improvements to the ROTHCON process

5. Perform testing to ensure proper functioning of Cicada coupling

6. Assess the VERA-CS CILC capability for full core model using Cicada and ROTHCON

2 CICADA API

Cicada development work for this milestone focused on delivering a pin-level interface to the coupled crud growth, oxide growth, and heat transfer capability to make it accessible from VERA-CS. The interface was designed to be a drop-in replacement for the DonGoose interface with additional inputs and outputs for the heat transfer and corrosion models. These models are documented in [5] and [9]. The details of this interface are outlined below.

2.1 Cicada Swarm Interface

The Swarm interface (accessed by included Cicada_Swarm.h) includes functions for initializing, finalizing, time stepping, setting model parameters, and accessing solution data on individual pins within the simulation. Like DonGoose, this C-language interface treats each pin in the model individually, allowing for individual specifications of geometry/mesh, material properties, and other model parameters, while allowing them to be initialized, finalized, and time stepped in unison.

2.1.1 Creating and Destroying a Swarm Instance

An instance of a swarm interface is managed through a handle (a pointer of type CicadaSwarm) which is subsequently used in all interface functions to apply changes to and extract data from the interface. A swarm instance is created using the create function:

CicadaSwarm∗ CicadaSwarm_create (MPI_Comm comm) ;

A handle to a valid MPI communicator is needed. The swarm will be created over this handle. When usage of the instance is completed, the destroy function must be called to clear any memory allocated by the instance.

void CicadaSwarm_destroy (CicadaSwarm∗ swarm) ;

The pointer passed to the CicadaSwarm˙destroy procedure will be NULL upon return from the function.

2.1.2 Crud Model Options

The DonGoose model option interface was directly exposed in the swarm interface to allow for compatibility with existing schemes for setting options in VERA-CS. Both double and integer typed options may be set on a given swarm instance via the following interface calls:

void CicadaSwarm_setCrudModelOptionInt (CicadaSwarm∗ swarm ,
                                        const int key_length ,
                                        const char key [ ] ,
                                        const int value) ;

void CicadaSwarm_setCrudModelOptionDouble (CicadaSwarm∗ swarm ,
                                        const int key_length ,
                                        const char key [ ] ,
                                        const double value) ;

If needed, options may also be cleared:

void CicadaSwarm_clearCrudModelOptions (CicadaSwarm∗ swarm) ;

2.1.3 Creating Pin Models

Pins are initialized before individual pin setting and boundary conditions can be applied. An initialization function is used to create a specified number of pins on the local MPI rank:

```
void CicadaSwarm_initialize( CicadaSwarm* swarm,
                             const int local_num_pin,
                             const int model_dimension );
```

In addition, the user specifies the model dimension of the pin. If a dimension of 1 is specified, a 1-dimensional (radial) heat transfer solver is used in the cladding model, while a value of 3 specifies a 3-dimensional model. It should be noted that, in the swarm interface, all pins are locally owned by the calling MPI rank: they do not span multiple MPI ranks.

Next is a sequence of functions that set model parameters for a given pin on the calling MPI rank. A given pin is specified by the parameter local_pin_id in each of the function signatures, and these local pin IDs use C-style indexing (i.e., they start at 0 and are less than local_num_pin). The mesh of each pin is specified via the following function:

```
void CicadaSwarm_setMesh( CicadaSwarm* swarm,
                          const int local_pin_id,
                          const double clad_outer_diameter,
                          const double clad_thickness,
                          const double outer_radial_zone_thickness,
                          const int outer_radial_zone_num_cells_r,
                          const int inner_radial_zone_num_cells_r,
                          const int num_cells_theta,
                          const int num_cells_z,
                          const double* axial_mesh );
```

Pin meshes are logically cylindrical and subdivided into radial, azimuthal, and axial zones. In the azimuthal (theta) direction, a number of cells is specified, and even subdivisions are applied around the circumference of the pins. In the axial (z) direction, a number of cells and an array of cell center positions is provided in the form of an axial mesh. In the radial direction, a number of parameters is needed to specify the geometry and mesh. The outer diameter of the clad and clad thickness give the radial dimensions of the cladding. The mesh in the radial direction is divided into two zones, an inner and an outer zone. The outer zone is intended to mesh the oxidized region of the cladding, while the inner zone is intended to mesh the region of clad material that does not oxidize, allowing the user to refine the mesh in the oxidation region. The thickness of the outer region is specified by a parameter, while the inner region thickness is defined implicitly. Hence, each radial zone has a fixed number of cells, with each cell of the same width. In a 3-dimensional heat transfer simulation, it is recommended to estimate the oxide thickness to determine the outer zone thickness and to use a larger number of mesh cells in this region. Fine mesh cells in the oxidation zone in a 3-dimensional simulation allow for a more accurate reconstruction of the oxide/metal interface temperature, which in turn gives a more accurate prediction of the oxide. In a 1-dimensional heat transfer simulation, the number of cells in the radial direction are unused, so a parameter of 1 can be passed. An example of how the clad/oxide mesh is set up in Cicada is given in Figure 1.

Material properties for each pin are given by the following function:

```
void CicadaSwarm_setCladData( CicadaSwarm* swarm,
                              const int local_pin_id,
                              const double clad_thermal_conductivity,
                              const double clad_density,
                              const double clad_specific_heat_capacity,
                              const double oxide_thermal_conductivity,
                              const double oxide_density,
                              const double oxide_specific_heat_capacity );
```

Both cladding material properties and oxide material properties are needed for the heat transfer solver. Parameters needed by the oxidation model can optionally be set by the following function:

```
void CicadaSwarm_setCorrosionModelData( CicadaSwarm* swarm,
                                        const int local_pin_id,
```
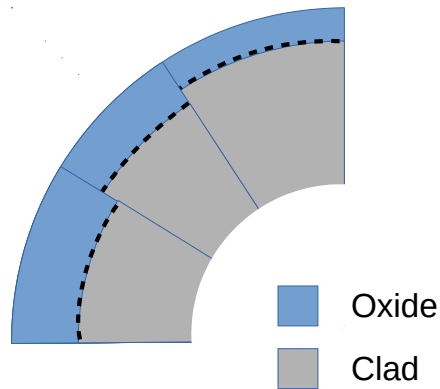
(a) Example of clad mesh when the 1D solver is used. An oxide and clad region are modeled for each sector. The oxide thickness is solved analytically, meaning there is no numerical error in determining the oxide thickness, but heat flows only in the radial direction.
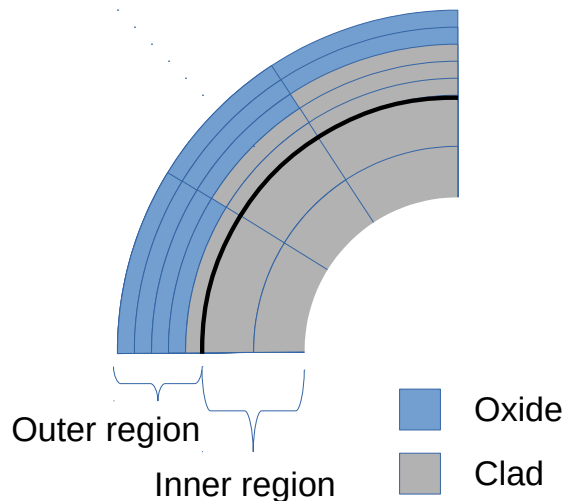
(b) Example of clad mesh when the 3D solver is used. The outer region thickness is fixed, and the solid black line represents the fixed division between inner and outer regions. The user sets the number of rings in the outer and inner region. As the oxide grows, rings in the outer mesh change from clad material to oxide material. The 3D mesh allows the oxide thickness to be nonuniform in the azimuthal direction. A fine mesh is required in the outer region to adequately resolve the interface between oxide and clad material.

Figure 1. How Cicada meshes the clad when using 1D and 3D solvers.

```
                                   const double R,
                                   const double k1 ,
                                   const double Q1,
                                   const double Q2,
                                   const double Q3,
                                   const double D3,
                                   const double E3 ,
                                   const double C0,
                                   const double M,
                                   const double P0 ,
                                   const double fast_flux  );
```

Calling this function is not required since a set of defaults is provided. The variables of the oxide model are documented in Section 3.3 and [9].

Once the pin mesh, materials, and oxidation model parameters have been set, the pins may be initialized via the pin create function:

```
void CicadaSwarm_createPin ( CicadaSwarm∗ swarm ,
                             const int local_pin_id ,
                             const int assembly_id ,
                             const int row_id ,
                             const int column_id  );
```

Here, a pin is assigned a VERA assembly ID and a row and column ID within that assembly. Pins must be initialized before setting boundary conditions and performing time integration.

2.1.4 Setting Boundary Conditions

Before every time step and after initialization, users can set boundary conditions. For the crud model, coolant data are set across the entire simulation in an manner identical to that used for the DonGoose interface:

```
void CicadaSwarm_setCoolantData ( CicadaSwarm∗ swarm ,
                                  const double inlet_temperature ,
                                  const double particulate_nickel_ferrite ,
                                  const double soluble_nickel ,
                                  const double soluble_iron ,
                                  const double soluble_boron ,
                                  const double soluble_lithium ,
                                  const double soluble_hydrogen  );
```

Pin-local thermal-hydraulic boundary conditions are set on individual faces given an azimuthal (j) and axial (k) index:

```
void CicadaSwarm_setBoundaryData ( CicadaSwarm∗ swarm ,
                                   const int local_pin_id ,
                                   const int j ,
                                   const int k ,
                                   const double heat_flux ,
                                   const double surface_temperature ,
                                   const double coolant_temperature ,
                                   const double tke ,
                                   const double tsat ,
                                   const double pres ,
                                   const double qboil  );
```

Here, the heat flux is given on the inner surface of the cladding, while the surface temperature, coolant temperature, turbulent kinetic energy, saturation temperature, coolant pressure, and heat flux due to boiling are given at the outer surface of the cladding. Boron absorption is set on the pin mesh faces separately:

```
void CicadaSwarm_setBoundaryBabs( CicadaSwarm* swarm,
                                  const int local_pin_id,
                                  const int j,
                                  const int k,
                                  const double babs );
```

2.1.5 Time Stepping

The time stepping algorithm consists of a total time step size and the number of substeps to perform within that time step:

```
void CicadaSwarm_step( CicadaSwarm* swarm,
                       const double time_step_size,
                       const int num_sub_step );
```

2.1.6 Accessing Solution Data

Solution data are accessed on each local pin and face:

```
void CicadaSwarm_getSolution( const CicadaSwarm* swarm,
                              const int local_pin_id,
                              const int j,
                              const int k,
                              double* crud_thickness,
                              double* crud_mass_density,
                              double* boron_mass_density,
                              double* crud_mass_evaporation,
                              double* crud_thermal_resistance,
                              double* oxide_thickness,
                              double* oxide_metal_interface_temperature,
                              double* oxide_thermal_resistance,
                              double* clad_inner_surface_temperature,
                              double* clad_thermal_resistance );
```

The solution data include data from the crud model, oxidation model, and thermal model. Note that individual thermal resistances are provided for the crud, oxide, and clad layers.

3   VERA-CS CILC CAPABILITY

3.1   ROTHCON Usability Improvements

The ROTHCON capability was initially developed and demonstrated for single-pin geometry in [10] because it was found that it was possible for the resolution of a rod surface T/H to have an impact on rod crud deposition [7]. This capability was then expanded to rod-bundle geometry in [11], and in [8] it was assessed for different operating conditions to demonstrate its applicability to different conditions from which the data were obtained. In these previous studies, however, enabling the feature in a CTF simulation was actually only available to the developer. This milestone set out to streamline the ROTHCON process so that VERA-CS users can employ it in their simulations.

An overview of how the ROTHCON process is employed is provided below:

1. The user runs a CFD simulation for a rod-bundle using the spacer grid to be used in the core-scale model. At least one or two spacer grid spans must be modeled to properly capture the flow behavior in the simulation results. A CFD simulation is needed for each spacer grid type that will be employed in the VERA-CS simulation; however, grid datasets are then reusable as long as the grid type does not change.

2. The user generates a grid data library for the reference span using the Reconstruct Python package originally developed in [11]. The grid data are added to a single grid library file.

3. The user links selected spacer grids in the VERA-CS common input file (VERAIn) file to datasets in the grid data file. This linkage is passed to CTF through the xml2ctf preprocessor utility.

4. During the simulation, CTF creates a rod surface coupling mesh that is more refined than the traditional CTF rod mesh and is used for coupling to MAMBA.

5. CTF uses the grid data file to calculate multipliers on the nominal TKE and heat transfer coefficient (HTC) for each face in the rod surface coupling mesh. The new HTC values, which represent the HTC shape predicted by CFD, are used to calculate the local rod surface coupling mesh temperature distribution. The new temperature and TKE distributions are passed off to MAMBA as boundary conditions.

Details of how the multiplier maps are formed and how the multipliers are applied to the CTF T/H solution on the rod surface are covered in detail in [10], [11], and [8]. Because ROTHCON was initially a research feature, Steps 2 and 3 were not originally designed to be production level. Originally, the user generated a text data file for each pin in the model and had to manually map each text file to each pin in the CTF model in Step 3, which is not practical for performing large-scale simulations. Also, the full pin-length data files had to be pregenerated using a set of Python tools for each model.

Step 2 in the process was previously accomplished by developing the Python Reconstruct utility, which is used to post-process CFD data to create rod surface multiplier maps for the pins in the model. As part of this milestone, Reconstruct was modified to generate a single grid data file from a selected reference grid span rather than a set of pin data files. The pin data are put into an HDF5 format file for better organization and compression of the data compared to the existing pin text files. The grid data file is reusable for models with different spacer grid placement, which eliminates the need to pregenerate a full pin-length data file.

An example of the file layout is shown in Figure 2. In the example, "MVGGRID" is the name of a reference grid. The file can contain multiple grid types. A grid directory contains "HTC" and "TKE" directories, which contain the pin HTC and TKE multiplier maps, respectively. There must be a dataset for each pin in the assembly. Each dataset is a two-dimensional (2D) array that takes the azimuthal location and axial location on the rod surface and returns a multiplier. The mesh that the data is given in the pin datasets is provided in the top-level "MESH" directory. It is a requirement that all grid types and pin datasets use the same mesh. Finally, the "pin_index" dataset in "MESH" defines the location of each pin in the model. The feature only supports square rod lattice geometry.

Step 3 of the ROTHCON workflow was improved by eliminating the need for the user to explicitly determine how the pin maps correspond to actual pins in the CTF model. The xml2ctf preprocessor was modified to look for a new optional argument to the grid input in the VERAIn file. Keeping with this example, the user would add "gridmap=MVGGRID" to the grid card in the VERAIn file. If xml2ctf finds this input, it will search for a file called "gridDataFile.h5" in the simulation directory. In that file, it searches for the "MVGGRID" directory and then begins to construct a new HDF5 file designed specifically for the model being created. The layout of this file is shown in Figure 3.
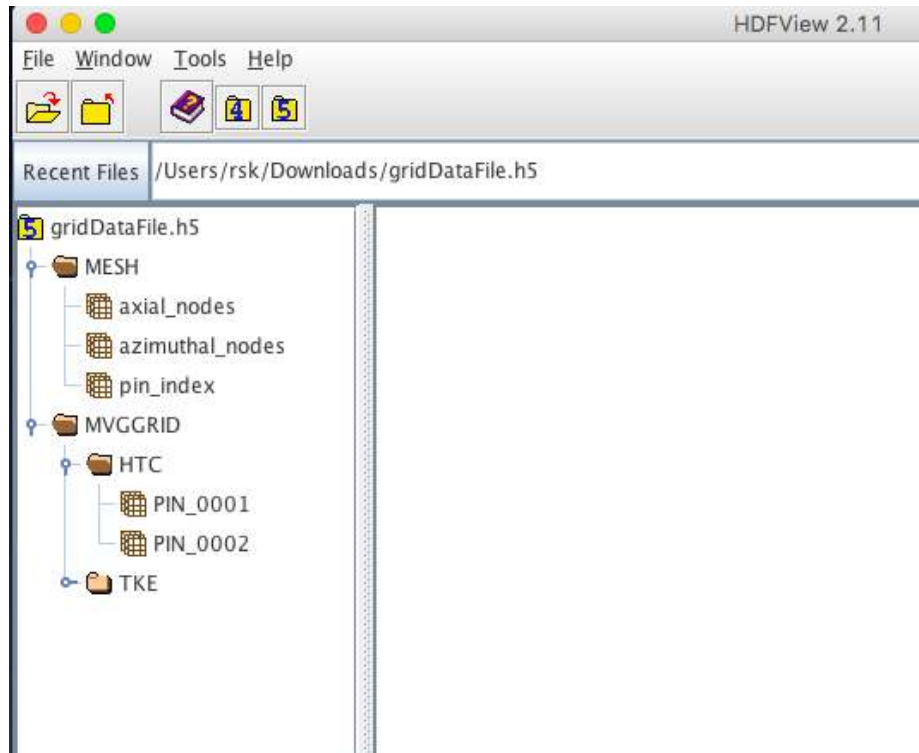
Figure 2. Example of a grid data file produced by Reconstruct and read in by xml2ctf

The pin multiplier maps are again divided into an "HTC" directory for HTC multiplier maps and a "TKE" directory for TKE multiplier maps. Each directory contains a dataset for every pin in the model. The number of pins can be in the tens of thousands for a full core model. Each dataset gives a 2D multiplier map. The top-level "MESH" directory provides the axial and azimuthal location of the multipliers in the pin datasets. Again, all pin multiplier maps in the model use the same mesh. In addition to creating the multiplier map file, xml2ctf will link every pin in the CTF model to a map in the multiplier map file.

To complete the streamlining of Step 3, CTF was modified to read in the single multiplier map HDF5 file. It reads in a multiplier map for each pin that has one specified and uses that in the coupling to MAMBA to reconstruct heat transfer and turbulence behavior on the rod's surface.

The preliminary ROTHCON process did not offer a straightforward means for obtaining coupling mesh reconstruction data. This was addressed by adding a "reconstruction" folder to the CTF native rod HDF5 file output. Each pin directory will have a "reconstruction" folder, and the folder will be populated with datasets that define the coupling mesh node locations, as well as datasets for the reconstructed temperature and crud solution.

3.2 Crud Coupling Refactor

To facilitate implementing a clad corrosion model into CTF and coupling with Cicada, the section of the code that couples to MAMBA was redesigned. Ultimately, the objective is to support two different methods for solving the clad chemistry (crud growth and deposition plus clad oxide growth): (1) use the existing direct coupling to MAMBA plus an internal oxide growth solver, or (2) use Cicada to handle the MAMBA coupling and oxide modeling. Both methods must work with the ROTHCON approach, and both will have similar interfaces.

The interface to MAMBA resided in a `Crud_driver` module previously; but now it is actually solving for clad chemistry. Therefore, the code was divided into three primary classes:

1. `CoreChemistry`
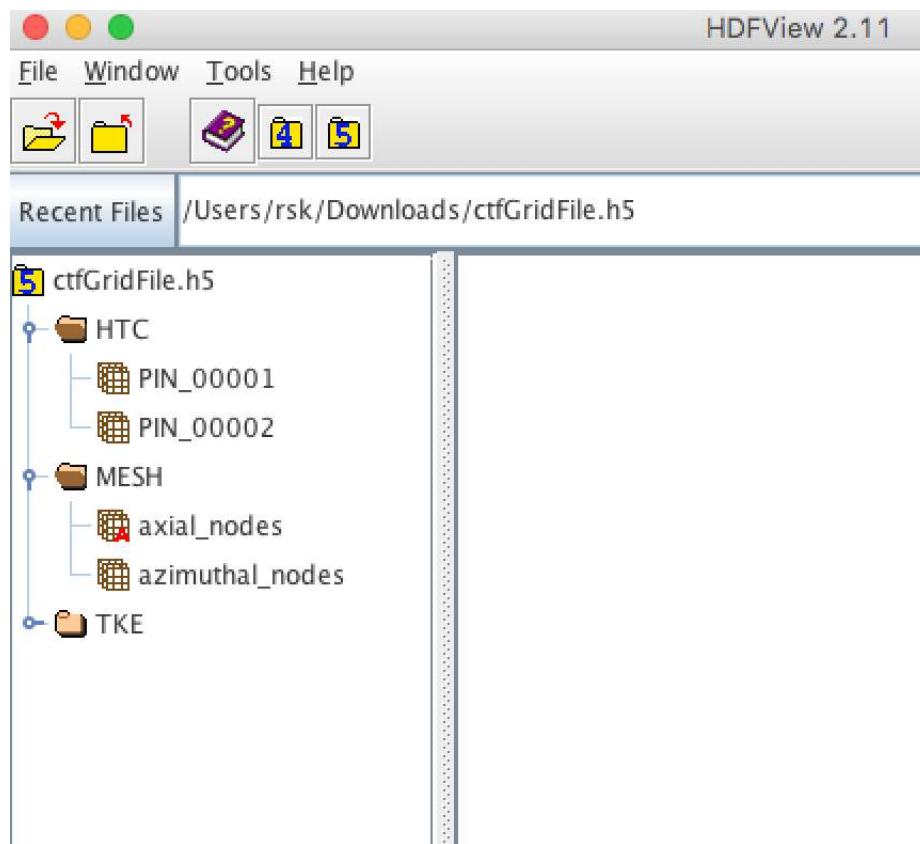
Figure 3. Example of a pin multiplier map file produced by xml2ctf and will be read in by CTF at execution.

2. `CladChemistry`

3. `ChemInterface`

Starting from the bottom, `ChemInterface` is an abstract class that defines the interface to the chemistry solver. It has two extensions: (1) `CtfCicadaInterface` is for the coupling to Cicada, and (2) `InternalChem` is the direct coupling to MAMBA plus the internal corrosion solver. This design allows the chemistry solver to be called in the same way from CTF without actually having to know what solver is being used. The `InternalChem` extension instantiates an object of a `CladCorrosion` class (discussed in Section 3.3), which performs the oxide growth solution. The oxide growth step is performed after the crud growth, but this all occurs inside the `InternalChem` solver without exposure to the caller.

The `CladChemistry` class is responsible for defining the coupling mesh, which may be more refined than the CTF mesh when using ROTHCON. It is also responsible for storing chemistry code boundary conditions data and solution data and for mapping CTF T/H data to the `ChemInterface` and mapping the `ChemInterface` solution back to CTF. One object of this class is instantiated for each pin, where clad chemistry will be solved in the model.

The `CoreChemistry` class is the manager for the `CladChemistry` objects and the `ChemInterface`. The boundary conditions are set, and the solution is obtained from the chemistry code on a per-pin basis, but other elements like the chemistry solve, rewind, restart, and initialization are performed once for all pins in the model. The manager class is therefore needed to store the pin objects and to drive setting and obtaining data while also driving the larger scale solution algorithm. Figure 4 shows the relationship of the classes in a graphical form.

The crud driver module still exists one more level up from the `CoreChemistry` class and is responsible for defining the overall solution logic such as determining what to do on the initial state versus subsequent states or when to set a restart point and when to rewind the solution. The module is also responsible for calculating the source term mass balance for providing coolant chemistry boundary conditions to the `ChemInterface`. It is envisioned that some of these tasks can be moved into the newer classes in the future for better encapsulation and comprehensibility.
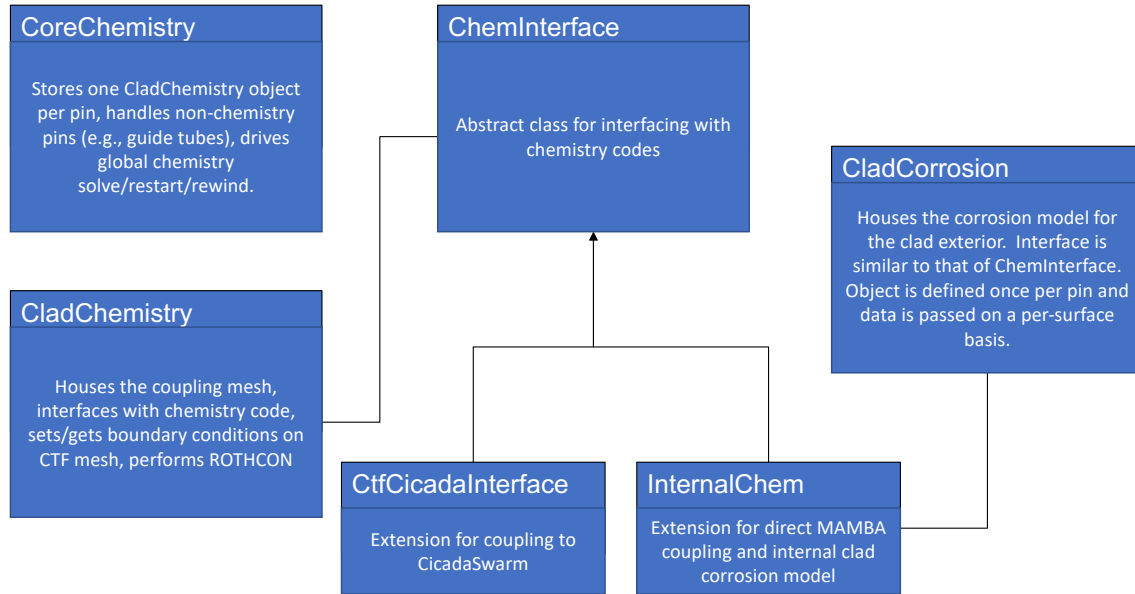
Figure 4. Class diagram for new classes created to handle the coupling of CTF and clad chemistry codes.

3.3 Implementation of Clad Corrosion Model

Prior to performing the coupling with Cicada, a clad corrosion model was implemented directly into CTF. The EPRI/KWU/C-E model described in [12] was used, which is the same model that was previously implemented into Cicada [5]. The model is a two-zone model that includes pre- and post-transition regions demarcated by a transition thickness. In the pretransition region, oxide growth follows a cubic rate law (Equation 1), and in the post-transition region, it follows a linear rate law (Equation 2). The transition thickness is defined by Equation 3

$$\frac{dS^3}{dt} = k_1 \exp\left(Q_1/(RT_{om})\right) \tag{1}$$

$$\frac{dS}{dt} = k_2 \exp\left(Q_2/(RT_{om})\right) \tag{2}$$

$$S_{\text{trans}} = D_3 \exp\left(Q_3/(RT_{om}) - E_3 T_{om}\right) \tag{3}$$

The coefficients, k_1, Q_1, Q_2, D_3, E_3, and R, are defined by the International Atomic Energy Agency [12] and repeated in Table 1. k_2 is a function of the fast flux as shown in Equation 4.

$$k_2 = C_0(1 + 3.22(M\Phi)_0^P) \tag{4}$$

The coefficients, C_0, M, P_0, and the approximation of the fast flux, Φ, are also provided in Table 1. The oxide thickness is S in microns, t is time in days, and T_{om} is the temperature at the oxide/clad interface in Kelvin. The T_{om} is calculated in the corrosion model using the default or user-provided oxide thermal conductivity. The clad surface heat flux is known, as well as the oxide thickness of the previous timestep, which allows for estimation T_{om} for growing oxide over the next timestep. It is possible to overshoot the transition thickness in a given timestep. If this happens, the code will back up and grow the oxide thickness to the transition point and then switch models to finish the timestep.

Table 1. Coefficients of the oxide corrosion model [12]

Coefficient	Value
R	$1.987\,\mathrm{cal\,mol^{-1}\,K^{-1}}$
k_1	$1.89 \times 10^{10}\,\mathrm{\mu m^3\,d^{-1}}$
Q_1	$32\,289\,\mathrm{cal\,mol^{-1}}$
Q_2	$27\,354\,\mathrm{cal\,mol^{-1}}$
D_3	$2.14 \times 10^7\,\mathrm{\mu m}$
E_3	$1.17 \times 10^{-2}\,\mathrm{K^{-1}}$
C_0	$8.04 \times 10^7\,\mathrm{\mu m\,d^{-1}}$
M	$7.46 \times 10^{-19}\,\mathrm{cm^2\,s\,n^{-1}}$
P_0	0.24
Φ	$9.0 \times 10^{14}\,\mathrm{n\,cm^{-2}\,s^{-1}}$

An addition was made to the model implemented into CTF, the effects of which will be shown in Section 4. EPRI materials discuss [13] that the coolant's lithium content can further accelerate the oxide layer growth, so a multiplier is defined for application to pretransition (Equation 5) and post-transition (Equation 6) regions.

$$F_{\mathrm{Li,pre}} = \exp(0.65 * (0.12l - 23.0l/T_{om})) \tag{5}$$

$$F_{\mathrm{Li,post}} = \exp(0.65 * (0.17l - 20.4l/T_{om})) \tag{6}$$

F_{Li} is a multiplier that is applied to the pre- and post-transition growth rates of Equations 1 and 2.

The `CladCorrosion` class discussed in Section 3.2 houses the corrosion model. The previously discussed `InternalChem` extension of the `ChemInterface` class houses one object per pin. The interface of the `CladCorrosion` class is similar to that of the chemistry code, in which the boundary conditions are set, and the solution is obtained on a per-surface basis. The solve, rewind, and restart setpoints are calculated once per pin and are called from the `ChemInternal` object.

3.4 Coupling to Cicada

Cicada offers a C-style interface called CicadaSwarm which was discussed in Chapter 2. The `CtfCicadaInterface` class (shown below) is a wrapper for the `CicadaSwarm` interface.

```
type, extends(ChemInterface) :: CtfCicadaInterface
    private
    !> The object that points to the Cicada interface
    type(c_ptr) :: cicadaSwarm = C_NULL_PTR
    !> Takes pin ID and returns the ratio of the outer clad
    !> radius to inner clad radius [ ]
    real, allocatable :: outerRadiusToInnerRadius(:)
contains
    procedure :: addPin => addPin_CtfCicadaInterface
    procedure :: setBoundaryData => setBoundaryData_CtfCicadaInterface
    procedure :: setCoolantData => setCoolantData_CtfCicadaInterface
    procedure :: setRestart => setRestart_CtfCicadaInterface
    procedure :: solve => solve_CtfCicadaInterface
    procedure :: rewindToRestart => rewindToRestart_CtfCicadaInterface
    procedure :: get => get_CtfCicadaInterface
```

```
#ifdef HAVE_COBRA_TF_MONGOOSE
        procedure :: getMAMBAPtr => getMAMBAPtr_CtfCicadaInterface
#endif
        procedure :: clean => clean_CtfCicadaInterface
    end type
```

The intrinsic Fortran module, `iso_c_binding`, is used to provide an interface between the different languages, with CTF being written in Fortran 2003 and Cicada being written in c++. The class variables include the pointer to the `CicadaSwarm` object that will be used to model all rods in the computational domain. CTF uses a domain-decomposition approach to parallelize the solution. A single `CicadaSwarm` object will be used for each CTF domain. The `outerRadiusToInnerRadius` array is needed to convert the clad's surface heat flux (which is the argument passed in to `setBoundaryData`) to clad inner heat flux. Clad outer heat flux is passed in to this procedure because it is required in the direct MAMBA coupling.

The `CtfCicadaInterface` object instantiation function is shown below.

```
type(CtfCicadaInterface) function init_CtfCicadaInterface(comm,
                             nPin,
                             dimensions,
                             mambaPL)
```

The `nPin` argument represents the number of pins in the swarm. Only fuel rods owned by the CTF solution domain are considered in the swarm. The `CoreChemistry` class keeps track of which pins require a chemistry solution and converts the CTF pin indices (which include ghost rods and guide tubes) to the chemistry indices. The `dimensions` argument will be either 1 (1D) or 3 (3D), and the `mambaPL` argument is a parameter list that represents the MAMBA block in the VERAIn file. The instantiation function will do three things:

1. Create the `CicadaSwarm` by calling `CicadaSwarm_create`

2. Set all options that were included in the MAMBA block of VERAIn by calling either `CicadaSwarm_setCrudModelOptionInt` or `CicadaSwarm_setCrudModelOptionDouble`

3. Initialize the `CicdaSwarm` interface by calling `CicadaSwarm_initialize`

Note that if new options are added in the MAMBA block in VERAIn, they will need to be added in `CtfChemInterface`, as well. This is a drawback, but it is required because the data type needs to be known to determine which Cicada procedure to call.

The `addPin` is called for each pin to create all pins in Cicada that require a chemistry solution. The procedure accomplishes three things:

1. Defines the pin geometry and mesh by calling `CicadaSwarm_setMesh`

2. Sets material properties by calling `CicadaSwarm_setCladData`

3. Creates the pin in Cicada by calling `CicadaSwarm_createPin`

The coupling mesh is used to define the pin mesh, meaning the ROTHCON process will be applied to the boundary conditions passed in to Cicada. The mesh options can be set in the COBRATF block of VERAIn, and they will be passed in to this code section. At this time, a single set of mesh options is set for the whole model, but Cicada does offer the flexibility to set the options on a per-pin basis. The variable names in VERAIn are `cicada_outer_radial_zone_num_cells_r`, `cicada_inner_radial_zone_num_cells_r`, and `cicada_outer_radial_zone_thickness`. These arguments have defaults of 100, 20, and 100 μm, respectively, and they will have no effect if a 1D solution is being performed.

The material properties are set as constants in Cicada. The clad's thermal conductivity and specific heat are set using the internal CTF properties for Zircaloy using the saturation temperature for pressurized water reactor (PWR) operating conditions. The clad density is set to the cold density of Zircaloy. The oxide thermal conductivity is set to a default of $1.5\,\mathrm{W\,m^{-1}\,K}$, which is roughly the average of the values given by the MATPRO and FRAP models given in [14], but it can be overridden by user input. The oxide density and specific heat are set to the Zircaloy values. The density and specific heat will have no impact because the crud solve is a steady state solution performed at each state point. Also, the clad's thermal conductivity will not impact the solution because it is currently not being implemented in the CTF rod thermal solution.

The `setCoolantData` procedure is called once for all pins at each statepoint to update core chemistry information and wraps the `CicadaSwarm_setCoolantData` procedure. The `setBoundaryData` procedure wraps the `CicadaSwarm_setBoundaryData` procedure and is used for setting boundary conditions on the coupling mesh. The `setRestart` and `rewindToRestart` are provided for consistency with the MAMBA coupling, but they do not perform anything in Cicada because they have not yet been implemented in Cicada due to a need for more in-depth refactoring. The `solve` procedure wraps the `CicadaSwarm_step` procedure, and the number of substeps is set to one. CTF has its own internal sub-stepping procedure that can be used for sub-stepping the chemistry code.

The `get` procedure wraps the `CicadaSwarm_get` procedure, and `clean` wraps `CicadaSwarm_destroy` and also cleans up after class internal data. The `getMAMBAPtr` procedure returns a NULL pointer because the Cicada interface currently does not allow for obtaining a pointer to the `CRUDPin` object from MAMBA. Some workarounds for this include directly calling DonGoose, which is actually a singleton, or exposing a Fortran procedure in Cicada that wraps the call to DonGoose to maintain consistency in only interacting with Cicada.

A summary of assumptions, simplifications, and limitations of the coupling are as follows:

1. Material properties for Zircaloy are used to define the clad.

2. Constant properties are used for clad and oxide.

3. The clad/oxide thermal conductivity is not incorporated in the CTF fuel rod thermal solution.

4. The dimension option (1D vs. 3D) as well as clad radial mesh options can be set core-wide only.

5. The solution rewind procedure is not yet implemented, but it will be addressed in future work.

6. It is not yet possible to obtain the `CRUDPin` object pointer through Cicada, which precludes performing crud restarts.

3.5 Input/Output Changes

Several new input parameters have been added to the VERAIn file to support CIPS and CILC analysis. Table 2 summarizes the new inputs that were added to the VERAIn file.

The following new datasets have been added to the output HDF5 file. Table 3 summarizes the new datasets that were added to the HDF5 file.

Table 2. Summary of new inputs in the VERAIn COBRATF block

Parameter	Description
hi2lo_sub_axial	Declares the number of sub-levels that will be created in the coupling mesh for each CTF axial level.
hi2lo_sub_theta	Declares the number of sub-sectors that will be created in the coupling mesh for each CTF sector.
model_corrosion	Used to enable and disable the corrosion model in the internal CTF model.
crud_details	When set to 1, more information pertaining to CIPS and CILC modeling is printed to the HDF5 file.
enable_corrosion_lithium	Used to enable and disable the lithium effect in the CTF internal corrosion model.
clad_corrosion_model	Used to select the corrosion material model for the CTF internal corrosion model (options include ZIRLO, Zircaloy, and M5 cladding).
oxide_thermal_conductivity	Overrides the default oxide thermal conductivity.
cicada_outer_radial_zone_num_cells_r	Overrides the default number of radial zones in the Cicada oxide layer.
cicada_inner_radial_zone_num_cells_r	Overrides the default number of radial zones in the Cicada clad layer.
cicada_outer_radial_zone_thickness	Overrides the defualt thickness of the oxide layer in Cicada.

Table 3. Summary of new datasets added to HDF5 file for CIPS and CILC analysis. All datasets are optional and are only printed when the "crud_detals" flag is set to "1" in the COBRATF block of the VERAIn file.

Dataset name	Description
pin_crud_chimney_heat_flux	The heat flux leaving the crud surface due to chimney boiling. This value is calculated by MAMBA.
pin_crud_inner_surface_temp	The temperature at the interface between the clad and crud layer.
pin_max_corrosion_clad_temp	The maximum temperature at the interface between the clad and corrosion layer over all azimuthal locations for a given rod level.
pin_min_corrosion_clad_temp	The minimum temperature at the interface between the clad and corrosion layer over all azimuthal locations for a given rod level.
pin_max_corrosion_thickness	The maximum corrosion layer thickness over all azimuthal locations for a given rod level.
pin_min_corrosion_thickness	The minimum corrosion layer thickness over all azimuthal locations for a given rod level.
pin_max_crud_thickness	The maximum crud layer thickness over all azimuthal locations for a given rod level.
pin_min_crud_thickness	The minimum crud layer thickness over all azimuthal locations for a given rod level.

4 ASSESSMENT

4.1 WEC 5×5 Model

4.1.1 Model description

The Westinghouse 5×5 rod bundle experiments were a series of electrically heated rod bundle experiments performed at the Columbia University Heat Transfer Research Facility in the 1980s. The facility was used as part of a previous CASL milestone that defined a process for meshing and modeling departure from nucleate boiling (DNB) in rod bundles [15]. The model generated during that milestone was used to develop the ROTHCON process for rod bundles [11]. It is also used in this milestone to help with assessing the Cicada coupling.

The 5×5 array included all rods of the same dimension; no guide tubes were included in the array. An example of the lateral geometry is shown in Figure 5. The facility walls contained rounded corners. The radial power distribution in the facility was nonuniform. Specific dimensions and pin power factors have been redacted from the figure. All bundle dimensions are available in the technical report on the facility [16].

The axial geometry of the assembly is shown in Figure 6. The model consists of five mixing vane grids in the heated length of the model. Grid spans lengths are consistent with lengths in actual PWR fuel assemblies, though the heated length is slightly shorter than that of a typical PWR. An example of the mixing vane grid is shown in Figure 7.

The STAR-CCM+ simulation data were used to generate the ROTHCON maps for nominal conditions in the facility in [11]. Those same maps are used in this report when the ROTHCON feature is enabled. Only the facility geometry was used for the assessments in this report. The power distribution and operating conditions were changed to suit the needs in the performed assessments.
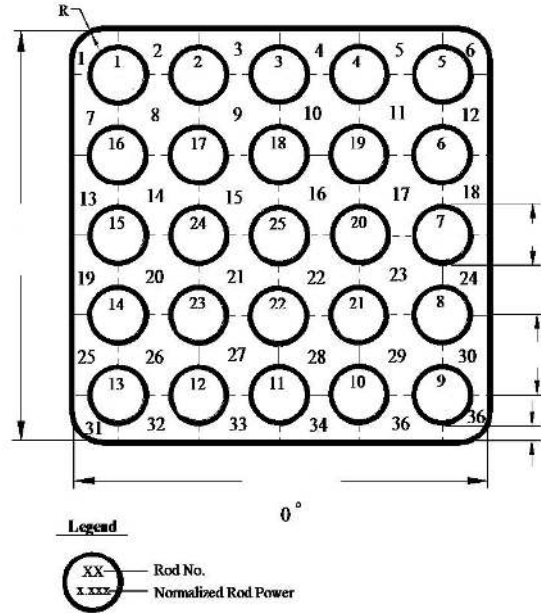
Figure 5. Lateral geometry of the 5 × 5 rod bundle geometry used in Westinghouse tests (reproduced from [16]).
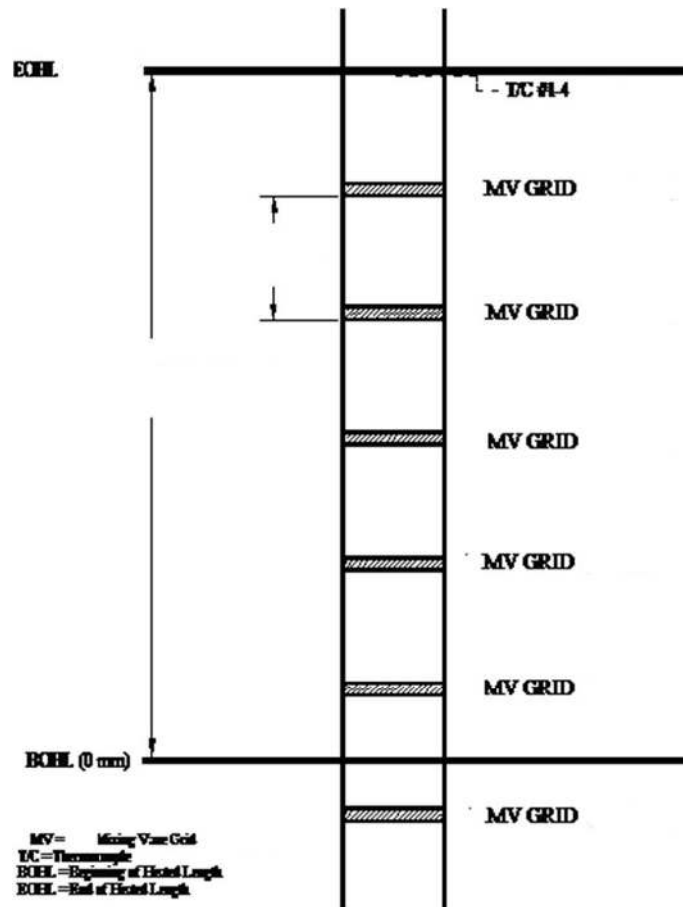
Figure 6. Schematic of axial design of Westinghouse 5 × 5 mixing vane grid facility (reproduced from [16]).
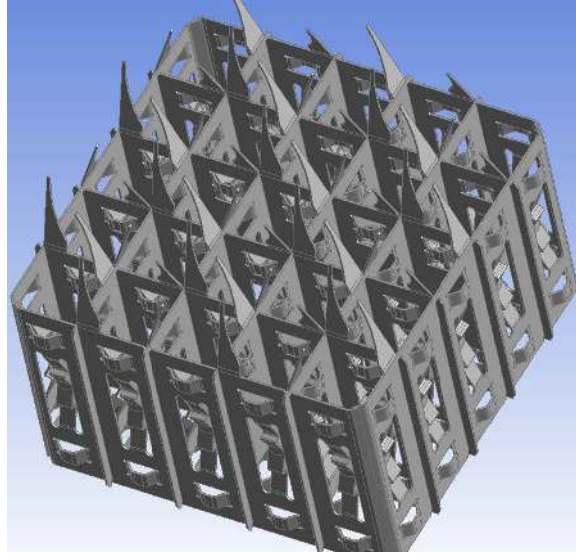
Figure 7. CAD representation of the mixing vane grid used in the 5×5 tests (reproduced from [16]).

4.1.2 Coupling mesh refinement

A coupling mesh refinement study was performed to verify that the agreement between the supplied HTC multiplier map continues to improve as the mesh is refined. The 5×5 rod bundle facility is used for the study. The ROTHCON HTC multiplier map that was generated for the facility is used as input to CTF. The coupling mesh refinement is denoted as $N \times M$ throughout the remainder of this report, where N is the number of divisions of a CTF rod sector into sub-sectors, and M is the number of divisions of a CTF rod level into sub-levels. CTF is run with coupling mesh refinement of 1×1 (no refinement), 2×2, 4×4, 8×8, and 16×16. CTF will perform a numerical integration of the supplied CFD data onto the coupling mesh faces. The coupling mesh multiplier map is then dumped to a file so it can be compared to the originally supplied map. The following comparison is done for the center rod in the 5×5 facility.

The supplied map has 64 azimuthal data points and 2,728 axial data points. This corresponds to 16 data points per CTF rod sector and over 50 data points per CTF axial rod level. The supplied map data are remapped to the coupling mesh, as shown in Figure 8.

| Supplied map data (available at vertices) Coupling mesh surface | Determine boundary node data using linear interpolation. Directly map supplied map nodes inside coupling mesh surface. | Assign weights to each node and perform weighted average: $M_c = 1/A_c \Sigma_{i=1}^{N} A_i M_i$ | A single multiplier is calculated for each coupling mesh surface |

Figure 8. Process for remapping supplied multiplier map data to coupling mesh.

The comparison is done by remapping the coupling mesh multipliers onto the supplied map mesh using a direct nearest neighbor interpolation. The root-mean-square error (RMSE) of the difference between all data points is then taken as shown in Equation 7, where N is the total number of data points in the supplied map (and remapped CTF coupling mesh map), and M is the multiplier. The results of the coupling mesh refinement are shown in Figure 9.

$$\text{RMSE} = \sqrt{\Sigma_{n=1}^{N}(M_{\text{CTF}} - M_{\text{supplied}})^2/N} \tag{7}$$

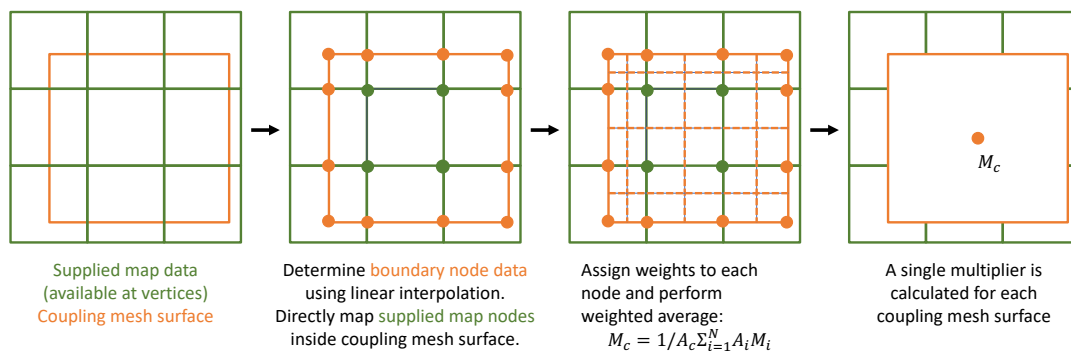The rate of improvement slows when moving to the 16×16 refinement because it is likely that substantial interpolation error begins to be incurred, as the coupling mesh size is on the order of the supplied data mesh. The improvement in the coupling mesh resolution of the supplied multiplier map can also be seen in Figure 10.

The multiplier map refinement comparison helps to verify that the mesh remapping is working correctly in CTF. An additional refinement study was performed in which the predicted CTF temperatures on the coupling mesh using the ROTHCON reconstruction are compared to the original STAR-CCM+ data that were used to generate the HTC multiplier map. The same refinement levels that were used for the multiplier map study are used for the temperature reconstruction study. Figure 11 shows the results. The results seem to asymptotically approach an error of 0.4–0.6 K. As shown in [8] and repeated here in Figure 12, the RMSE of the difference between CTF and STAR-CCM+ channel fluid temperature predictions is about 0.5 K. The fluid temperature will have a direct impact on predicted rod surface temperature, so this error will limit the degree to which the rod surface temperature predictions may be improved. Rods 5 and 13 are corner rods (shown in blue in Figure 12) that have experienced larger-than-average errors in fluid temperature prediction, which explains their less improved behavior.
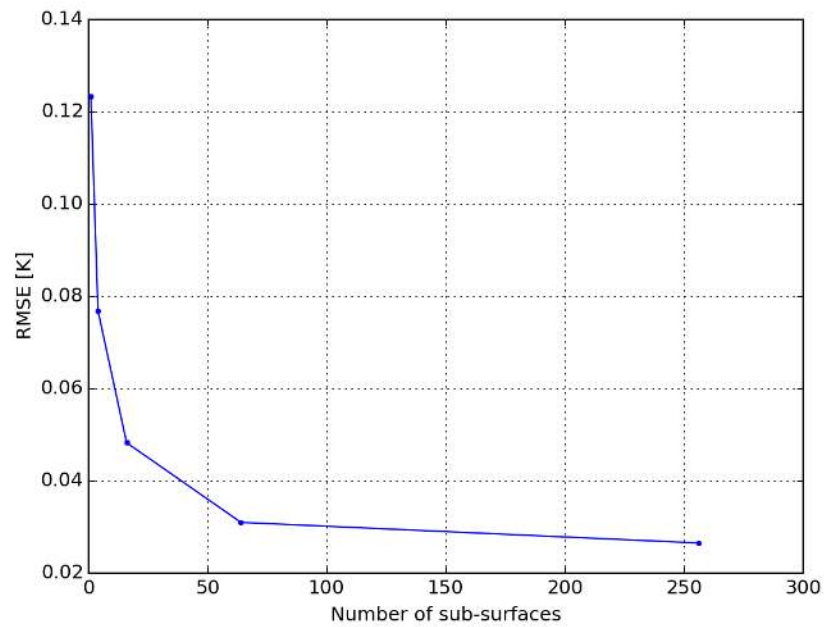
Figure 9. RMSE of the differences between the coupling mesh multiplier map and the multiplier map supplied to CTF. The results show that the error between the two maps continues to reduce as the coupling mesh is refined, and the results also confirm the expected behavior of the ROTHCON process.
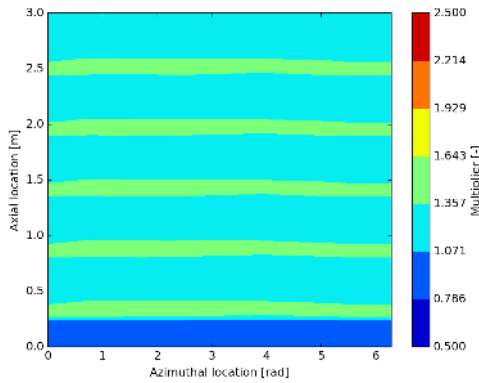
(a) Coupling mesh multiplier map using 1×1 refinement
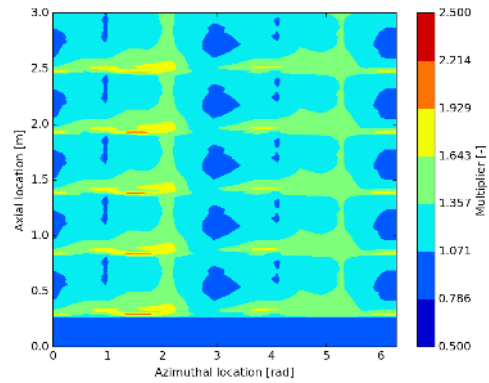
(b) Coupling mesh multiplier map using 4×4 refinement
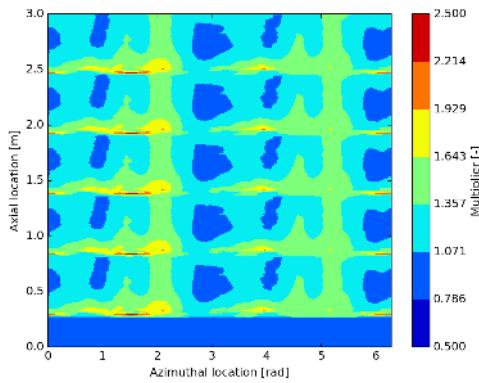
(c) Coupling mesh multiplier map using 16×16 refinement
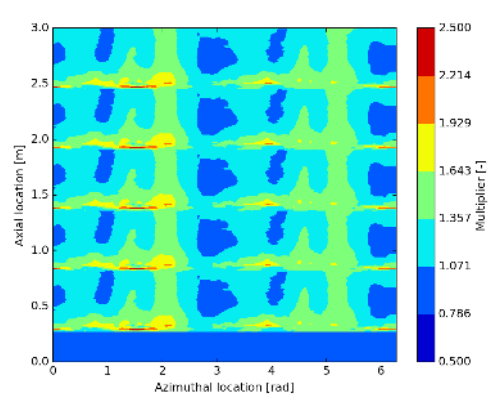
(d) Supplied multiplier map

Figure 10. Comparison of supplied map and coupling mesh map for HTC multiplier
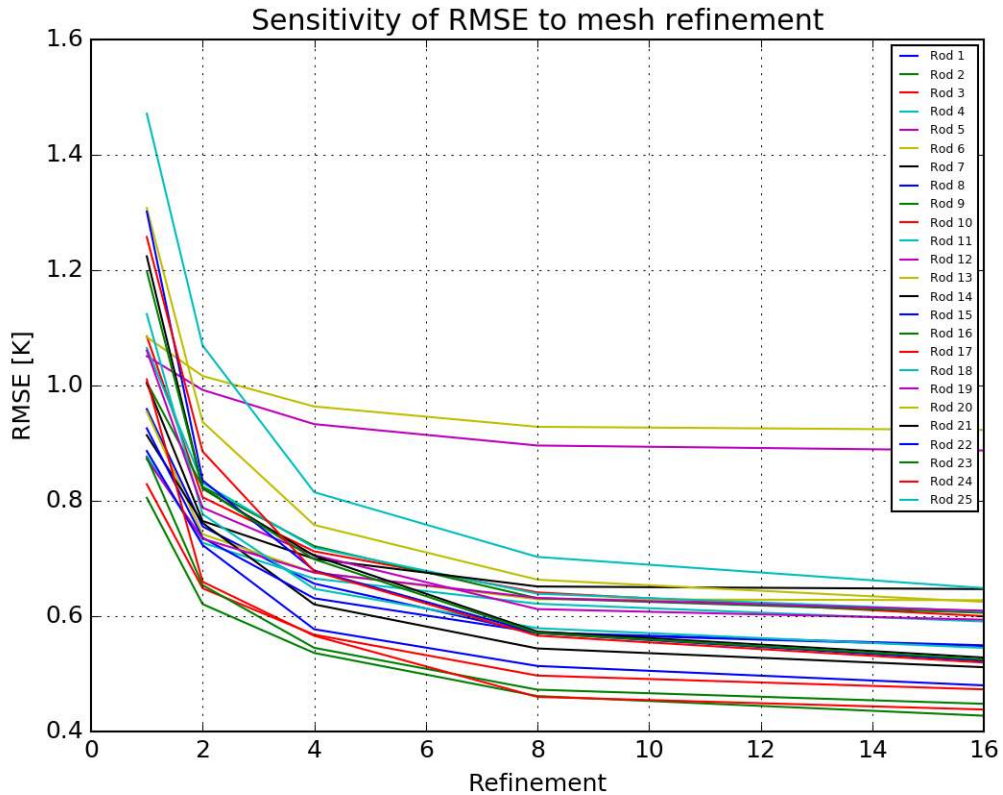
Figure 11. RMSE of the difference between STAR-CCM+ rod surface temperature predictions and CTF rod surface temperature predictions using the ROTHCON process. A single RMSE is calculated for each rod at each level of coupling mesh refinement. Adjacent subchannel temperatures of corner rods 5 and 13 compare less favorably with STAR-CCM+, leading to less of an improvement for those rods. The RMSE of the difference between CTF and STAR-CCM+ channel temperature predictions is $0.5\,\mathrm{K}$, which limits how well the results will match.
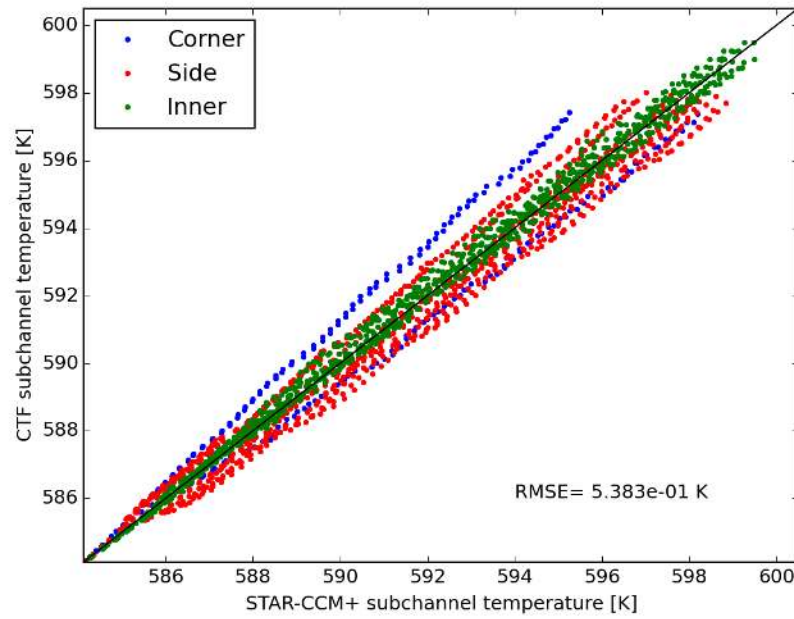
Figure 12. **Comparison of CTF channel temperatures and flow-weighted average of STAR-CCM+ fluid temperatures.**

4.1.3 Cicada coupling verification

The Cicada coupling was verified by running the 5×5 model using the two coupling options (existing internal coupling vs. the Cicada coupling) and comparing the results. The 1D-radial conduction option is used in Cicada, which makes the crud and corrosion solution steps essentially the same between the two approaches. The 5×5 case is run over a 360-day depletion divided into 360 steps. Coolant chemistry is held steady at the values given in Table 4.Thermal hydraulic conditions are held constant at nominal PWR conditions, and a uniform power distribution is used. The ROTHCON feature is used with two refinement levels: no refinement, and 2×3.

The maximum observed crud and corrosion thicknesses discrepancies between the two different coupling approaches for the case with no refinement are $0.08\,\mu m$ and $0.03\,\mu m$, respectively. The maximum observed crud and corrosion thickness discrepancies for the case with refinement are $0.15\,\mu m$ and $0.03\,\mu m$, respectively. The maximum crud and corrosion thickness for this simulation are about $35\,\mu m$ and $8\,\mu m$. This confirms good agreement between the two approaches and gives confidence that the coupling was implemented correctly.

Table 4. Coolant chemistry for the coupling verification test

Parameter	Value
boron	1000 ppm
lithium	3.0 ppm
soluble iron	0.915 ppb
soluble nickel	0.25 ppb
particulate nickel	2.2 ppb
hydrogen	$32.0 \cdot 10^{-6}$

4.1.4 Corrosion model sensitivity

It is known that crud's lithium content can have a significant impact on the rate of oxide layer growth. The author of the corrosion model that was implemented into Cicada and CTF included growth rate multipliers to capture the effects of lithium, which were discussed in Section 3.3. Crud lithium concentration is calculated by MAMBA, and the coupling interface simply needed to be expanded to expose this data. The multipliers were added to the internal CTF model to test the sensitivity of growth rate to this term.

The oxide thermal conductivity is another parameter that was investigated. As shown in Figure 13, which is reproduced from [14], there is a fairly large uncertainty in the thermal conductivity of the oxide layer. Different models produce values ranging between about 0.3 and $2.0\,\mathrm{W\,m^{-1}\,K}$ in most cases. While the spread of the models is large, an individual model does not seem to predict a strong dependence on temperature. Currently, the oxide's thermal conductivity is defaulted to $1.5\,\mathrm{W\,m^{-1}\,K}$, which is roughly the average of the MATPRO and Adams models; however, this value is exposed to the user in the VERAIn file, as well. The sensitivity of oxide growth was tested by reducing this value to $1.0\,\mathrm{W\,m^{-1}\,K}$.

The 5×5 bundle was run for 4 different cases in all: (1) nominal, (2) nominal with lithium effect enabled, (3) nominal with oxide thermal conductivity reduced, and (4) nominal with both lithium effect enabled and thermal conductivity reduced. The axial oxide thickness distributions for the four cases are shown for the pin with the thickest oxide growth in Figure 14. As the figure indicates, the lithium effect is significant and must be considered in the model. The oxide thermal conductivity can also have a significant impact on oxide thickness, especially when combined with the lithium effect. As the model dictates, the rate of oxide growth increases as the oxide layer gets thicker.
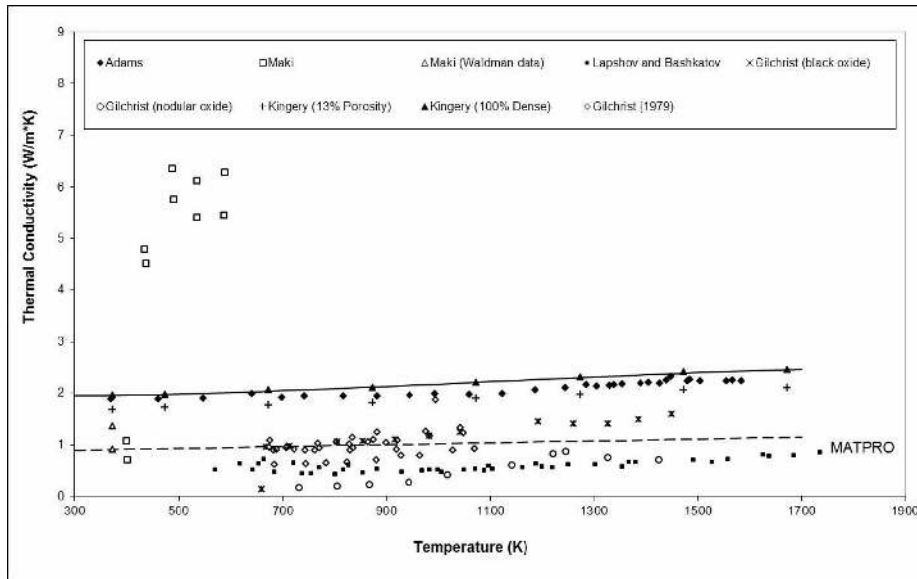
Figure 13. Oxide thermal conductivity predictions using different prominent models (Reproduced from [14]).
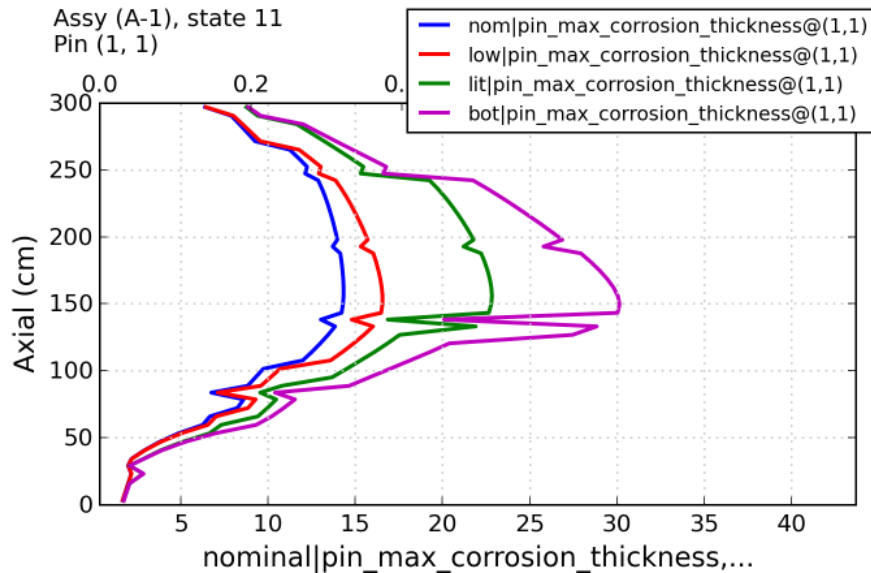
Figure 14. Sensitivity of axial oxide thickness to lithium effect and oxide thermal conductivity. The blue line is the nominal case, the red line is the nominal case with oxide thermal conductivity reduced from $1.5\,\mathrm{W\,m^{-1}\,K}$ to $1.0\,\mathrm{W\,m^{-1}\,K}$, the green line is the nominal case with the lithium effect turned on, and the purple line is the nominal case with both the lithium effect and the lowered oxide thermal conductivity.

4.1.5 Cicada equation dimensions

A primary benefit of coupling to Cicada is that it provides a fully 3D formulation of the thermal conduction solution in the clad and oxide layer. This can be important when oxide growth is nonuniform, because heat transfer will take the path of least resistance and will go around thicker oxide regions. This will lead to smaller temperature increases over those thick oxide regions when compared to using a 1D approximation, where the heat transfer is forced through the thick oxide region. Therefore, overall oxide growth will be smaller for the 3D case compared to the 1D case.

To assess the effect of the solution dimension, the 5×5 case was run for nominal conditions using a 1D solution and the 3D solution with various levels of mesh refinement. When using the 3D solve, the refinement of the clad and oxide mesh becomes important. The 1D case is just an analytical solution, so the clad and oxide regions are not actually meshed. Figure 1 gave an example of how Cicada meshes the clad and oxide regions. For this study, the mesh refinements are shown in Table 5.

The maximum bundle corrosion thickness for the mesh and solver combinations is shown in Figure 15. As the figure shows, the maximum corrosion thickness obtained with the 3D case is slightly less than the 1D case, as expected. For thicker corrosion, the difference between 1D and 3D will likely be larger due to the nonlinear growth rate of the oxide. The 3D results seem to be sufficiently converged when using 100 rings, and the simulation walltime is only slightly larger than the 1D case. While this study used an equal number of rings in the clad and oxide regions, it is likely that no more than 20 rings are needed in the inner region, so the walltime for a converged 3D case can be further reduced.

Table 5. Solver and meshing options for the assessment of corrosion sensitivity to using the 1D or 3D solver in Cicada.

Mesh number	Solver	Number of inner rings	Number of outer rings
1	1D	—	—
2	3D	1	1
3	3D	10	10
4	3D	100	100
5	3D	500	500
6	3D	750	750
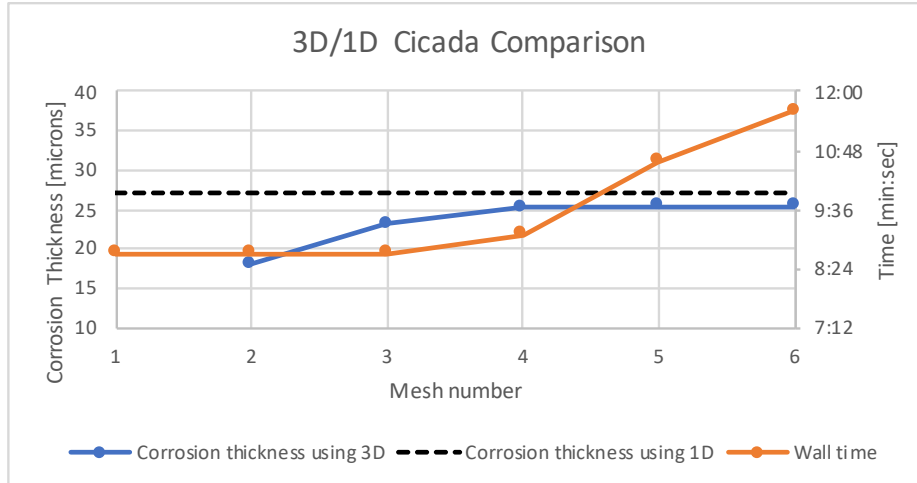
Figure 15. **Comparison of maximum bundle corrosion predicted using 1D and 3D Cicada for different mesh refinements. The wall time of each mesh/solver option is also shown. Mesh 1 is the 1D case. The corrosion thickness predicted by the 1D solution is shown with the horizontal dashed line to make for easier comparison with the 3D approach. The 3D case using 100 rings in the inner and outer regions appears to be sufficiently converged, and the wall time is only nominally larger than the 1D case and the coarser meshes in the 3D cases.**

4.1.6   Crud/Corrosion sensitivity to ROTHCON mesh

The effect of the ROTHCON process on maximum crud and corrosion growth is tested by running the 5×5 for a cycle depletion at different levels of coupling mesh refinement. The coolant chemistry conditions are set as shown in Table 6. The axial power distribution was taken from a fresh fuel bundle rod in a previous VERA-CS simulation and is shown in Figure 16. The radial power shape is set by applying a radial peaking factor of 1.15 to the inner 9 rods in the assembly. The nominal linear heat rate is set to $18.26 \, \mathrm{kW \, m^{-1}}$, with a bundle peaking factor of 1.7 applied. The highest peaking factor experienced in the bundle is 2.7. The simulation is run for four different ROTHCON coupling mesh refinements. The coupling mesh refinements in this study include 1×1, 2×2, 4×4, and 8×8. Figures 17–19 show the results of the refinement study.

Figures 20a–20d show the change in the pin surface corrosion thickness as the ROTHCON coupling mesh refinement is increased from 1×1 to 8×8. In the 1×1 case, the corrosion thickness is more spread out over the rod surface, and the maximum value is around $30 \, \mu\mathrm{m}$. Upon refining the coupling mesh to 8×8, streaks of corrosion thickness can be seen on the rod surface, and the maximum thickness increases to $50 \, \mu\mathrm{m}$. These results indicate that resolving the rod surface heat transfer and TKE behavior caused by rod bundle and spacer grid geometry may be important to properly resolving crud and corrosion growth that will affect CILC.

Table 6. Coolant chemistry conditions for the study on crud and corrosion thickness sensitivity to ROTHCON coupling mesh refinement.

Day	B [ppm]	H [m³/kg]	Li [ppm]	Ni_{sol} [ppb]	Ni_{par} [ppb]	Fe_{sol} [ppb]
0	1000	$3.75 \cdot 10^{-5}$	1.5	0.55	1.5	0.815
4	1000	$3.75 \cdot 10^{-5}$	1.5	0.55	1.5	0.815
12	1281	$3.75 \cdot 10^{-5}$	1.5	0.55	1.5	0.815
100	800	$3.75 \cdot 10^{-5}$	1.5	0.55	1.5	0.815
150	700	$3.75 \cdot 10^{-5}$	1.5	0.55	1.5	0.815
200	600	$3.75 \cdot 10^{-5}$	1.5	0.55	1.5	0.815
250	500	$3.75 \cdot 10^{-5}$	1.5	0.55	1.5	0.815
300	500	$3.75 \cdot 10^{-5}$	1.5	0.55	1.5	0.815
350	400	$3.75 \cdot 10^{-5}$	1.5	0.55	1.5	0.815
400	350	$3.75 \cdot 10^{-5}$	1.5	0.55	1.5	0.815
450	100	$3.75 \cdot 10^{-5}$	1.5	0.55	1.5	0.815
500	10	$3.75 \cdot 10^{-5}$	1.5	0.55	1.5	0.815
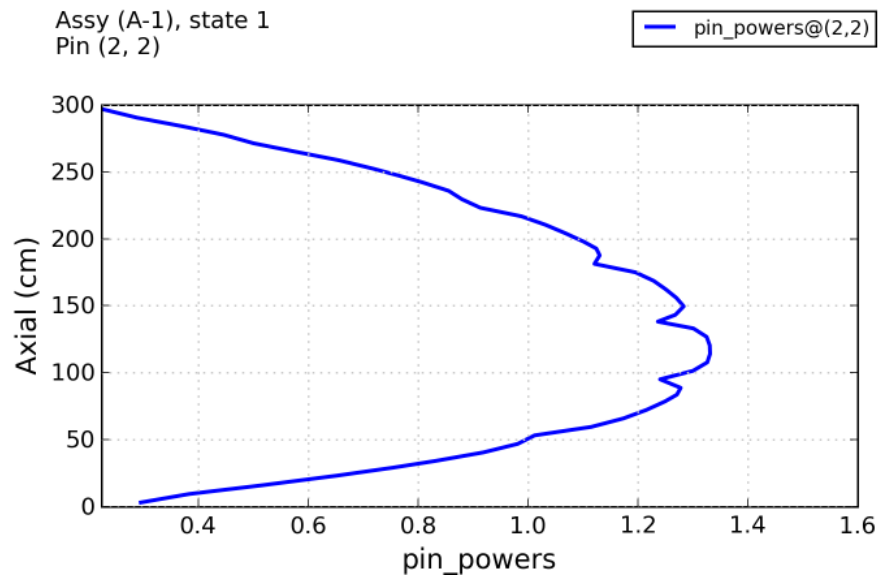
Figure 16. Axial power shape applied to all rods in the 5×5 bundle for the sensitivity study on crud and corrosion thickness to the ROTHCON mesh.
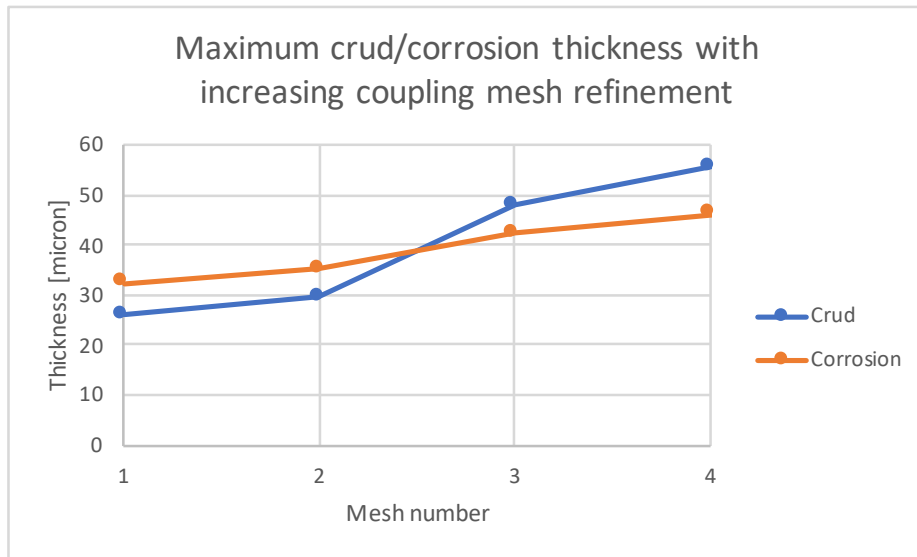
Figure 17. Change in the maximum crud and corrosion thickness in the 5×5 bundle as the ROTHCON coupling mesh is refined. Results are shown at the end of the depletion. Both the crud and corrosion maximum thickness increase as the coupling mesh is further refined. As the mesh is refined, low heat transfer regions are better resolved, which leads to higher temperatures and thicker crud growth. The higher temperature and larger thermal resistance of the crud leads to more oxide growth.
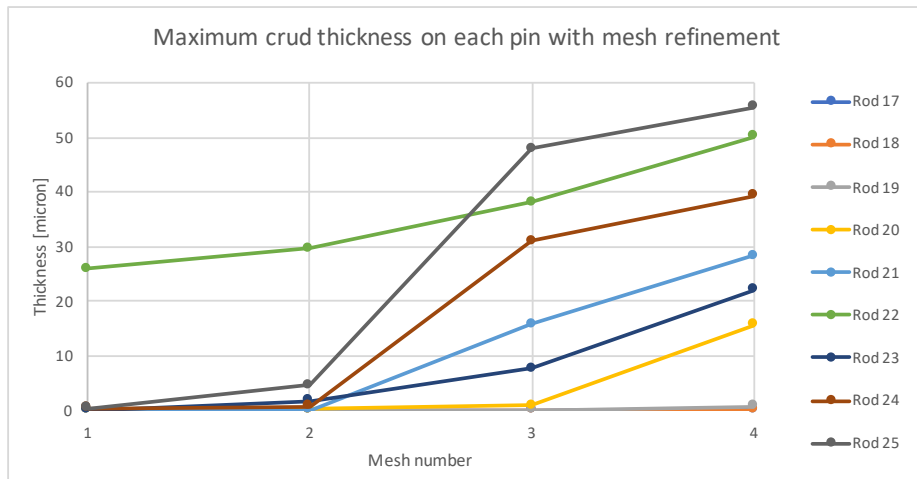
Figure 18. Change in the maximum crud thickness for each of the 9 inner pins as the ROTHCON coupling mesh is refined. Results are shown at the end of the depletion. At 1×1 refinement, most of the rods experience zero crud growth, but as hot spots are resolved and temperature rises above the saturation point, most rods begin to experience crud growth. As refinement is increased, the rod experiencing the maximum crud thickness switches from Rod 22 to Rod 25.
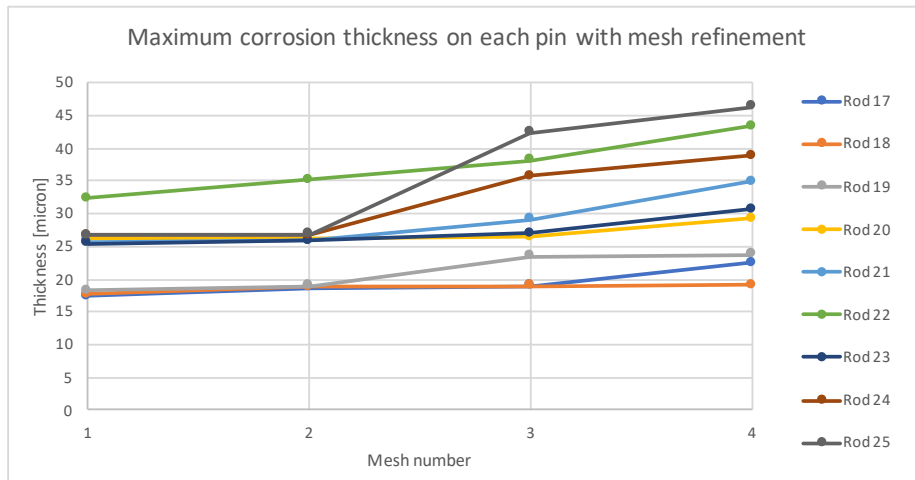
Figure 19. Change in the maximum corrosion thickness for each of the 9 inner pins as the ROTHCON coupling mesh is refined. Results are shown at the end of the depletion. As the coupling mesh is refined, all rods experience an increase in maximum corrosion, and the rod with the maximum switches from Rod 22 to Rod 25.
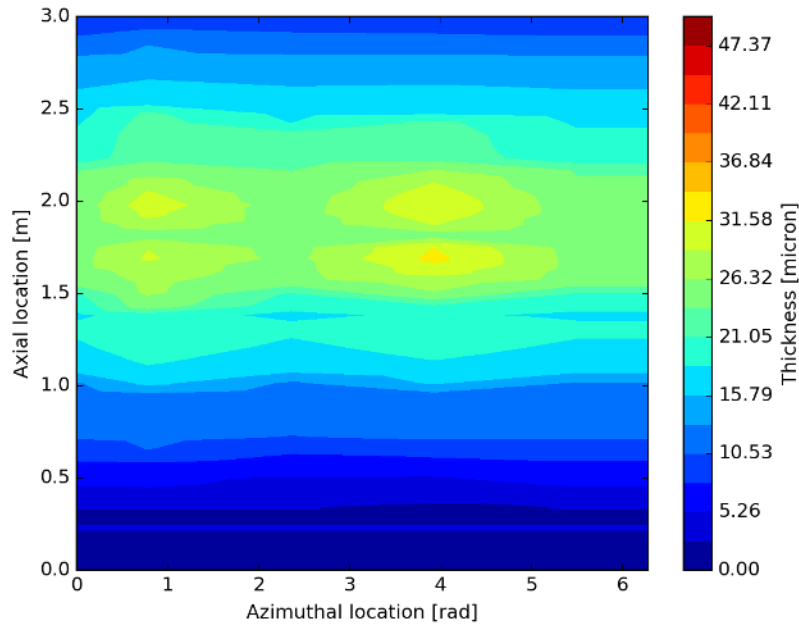
(a) **Pin surface corrosion distribution using 1×1 ROTHCON refinement.**
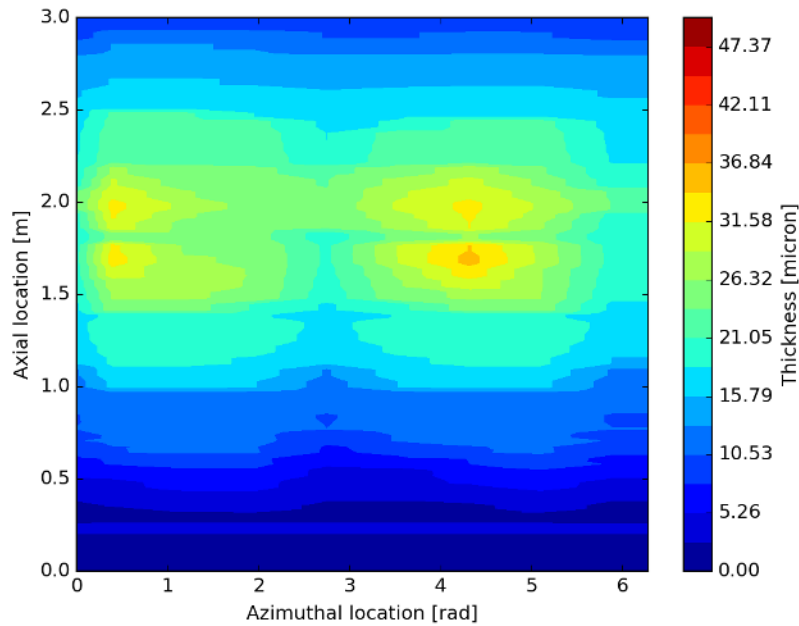
(b) **Pin surface corrosion distribution using 2×2 ROTHCON refinement.**

Figure 20. Pin surface corrosion distribution for different levels of ROTHCON coupling mesh refinement.
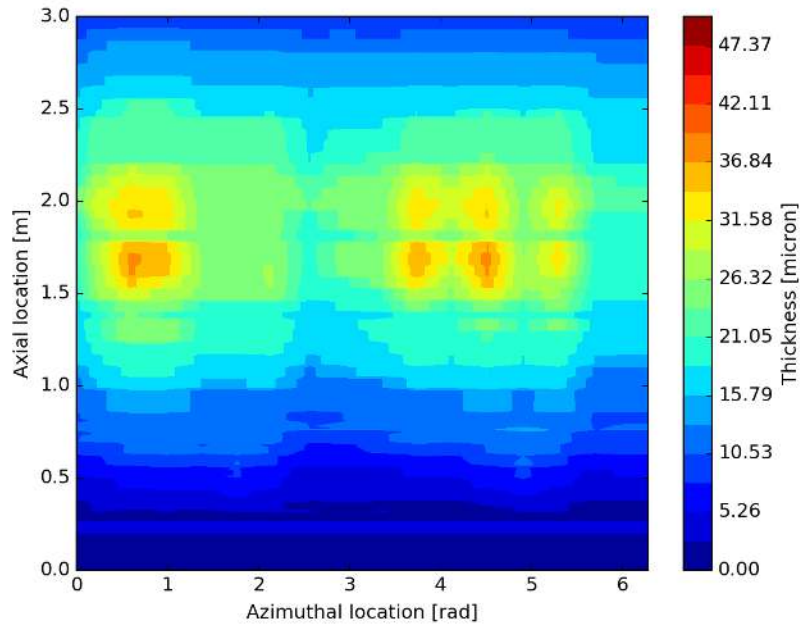
(c) Pin surface corrosion distribution using 4 × 4 ROTHCON refinement.
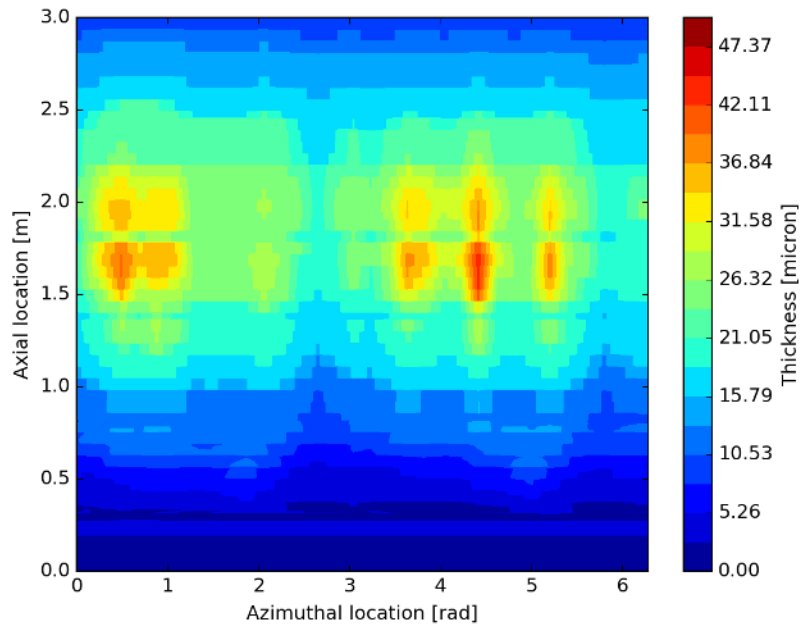
(d) Pin surface corrosion distribution using 8 × 8 ROTHCON refinement.

Figure 20. Pin surface corrosion distribution for different levels of ROTHCON coupling mesh refinement (continued).

4.2 Seabrook Nuclear Station

The Seabrook Nuclear Power Plant has one unit that is a Westinghouse 4-loop PWR design. The Seabrook Station is owned by NextEra Energy Resources and is located in Seabrook, New Hampshire. A 40-year operating license was granted in March of 1990 and expires in March of 2030. Seabrook Station is currently licensed for 3,648 MW_{th}, generating 1,244 MW electrical. The reactor core utilizes 193 Westinghouse 17×17 design fuel assemblies that house 264 fuel rods containing uranium oxide pellets enriched between 3 to 5 percent ^{235}U. The fuel assemblies contain 24 guide tubes and a central instrument tube. The active fuel region is 12 feet tall, including the fuel blanket regions. During each cycle, approximately one-third of the fuel is replaced with new fuel during the power outage.

4.2.1 Seabrook Cycle 5

Seabrook cycle 5 operated from December 1995 to May 1997. The VERA model and simulations for this work are performed on this cycle. Cycle 5 is of interest for CILC analysis because it experienced both core-wide CIPS and CILC failures of five fuel rods.

Cycle 5 was the first cycle in which multiple changes were made that may have added to increasing crud risk. The fuel assemblies had begun transitioning to a new fuel design, the Westinghouse V5H design without intermediate flow mixing grids, from the Westinghouse Standard fuel. Cycle 5 was the first cycle in a planned transition from 18- to 24-month cycles. Cycle 5 operated for about 502 effective full power days (EFPD).

Cycle 5 experienced axial offset due to CIPS. A sharp rise in reactor coolant fission products was measured in December 1996, indicating breach of cladding and fuel rod failure. Post-cycle fuel assembly examinations identified five failed fuel rods and documented the characteristics of the crud present on the rods. Multiple crud measurements were made for both failed and non-failed rods. All failed rods were adjacent to guide tubes and contained integral fuel burnable absorber integral fuel burnable absorber (IFBA). IFBA is a thin coating of ZrB_2 on the outside radius of the fuel pellet that is designed to absorb a limited amount of neutrons and regulate local power peaking for a time until the boron is depleted and the absorber effect disappears. The five failed rods were in four separate assemblies that contained fresh fuel. The fresh fuel assemblies are generally characterized with the highest power factors throughout the cycle.

4.2.2 Cycle 5 VERA Model Description

The VERA models for Seabrook cycle 5 were created from data provided previously by Westinghouse. The models were developed originally in previous CASL work and are shown in more detail in [6].

The work performed in this study focuses on the crud and corrosion growth to simulate CILC. The pin powers were calculated previously with a VERA-CS simulation and used as an input to the CILC simulations with coupled thermal hydraulics (CTF) and chemistry (MAMBA) codes. The Seabrook cycle 5 model was quarter core symmetric, with 51 axial regions that captured the fuel assembly grids and other material boundaries. The core was partitioned radially by the assembly. This required 193 cores for a few hours, depending on the resolution of the simulation. The Oak Ridge National Laboratory (ORNL) CADES computing cluster was used to perform the simulations.

Plant operations data were limited, so the cycle 5 simulations were performed at nominal all rods out hot full power conditions. Table 7 shows the statepoint dependent inputs used for cycle 5.

No measured data were available for the coolant chemistry, so the corrosion product concentrations were taken from the output of calculations run by the industry standard chemistry code, BOA. The coolant corrosion product concentrations are currently entered by statepoint and are shown in Table 7.

Table 7. Summary of VERA chemistry inputs for Seabrook cycle 5 simulations.

Statepoint	EFPD	H [m^3/kg]	Li [ppm]	Ni$_{sol}$ [ppb]	Ni$_{par}$ [ppb]	Fe$_{sol}$ [ppb]
1	0.0	3.20E-05	2.150	0.192	2.041	1.795
2	3.9	3.20E-05	2.150	0.192	2.043	1.795
3	13.0	3.20E-05	2.150	0.197	2.102	1.809
4	26.1	3.20E-05	2.150	0.198	2.159	1.788
5	38.1	3.20E-05	2.150	0.197	2.199	1.766
6	48.1	3.20E-05	2.150	0.337	3.667	6.593
7	48.2	3.20E-05	2.150	0.337	3.670	6.593
8	48.4	3.20E-05	2.150	0.195	39.470	1.741
9	48.6	3.20E-05	2.150	0.195	2.335	1.734
10	52.0	3.20E-05	2.150	0.336	3.865	3.163
11	78.2	3.20E-05	2.150	0.190	2.619	1.733
12	104.3	3.20E-05	2.150	0.186	2.523	1.699
13	156.4	3.20E-05	2.150	0.187	2.441	1.673
14	208.5	3.20E-05	2.150	0.184	2.370	1.683
15	260.7	3.20E-05	2.150	0.182	2.352	1.721
16	312.8	3.20E-05	2.150	0.179	2.367	1.792
17	364.9	3.20E-05	2.150	0.177	2.413	1.910
18	417.0	3.20E-05	2.000	0.176	2.484	2.057
19	477.0	3.20E-05	1.184	0.175	2.557	1.998
20	501.6	3.20E-05	0.850	0.175	2.626	1.949

The CFD data specific to the grid design used in Seabrook cycle 5 were not available. In order to test and demonstrate the CILC capability using the ROTHCON process for quarter core models, a proof-of-concept grid data map for a 17×17 fuel assembly was generated from the Westinghouse Electric Company (WEC) 5×5 CFD data. Nine rods from the 5×5 CFD data were taken and constructed in a symmetric pattern to create the 17×17 grid data maps. Figure 21 shows the arrangement of the indices of the pins used from the 5×5 model.

The 17×17 grid data map contains dummy data and does not represent the real thermal hydraulic conditions inside the cycle 5 fuel assemblies. However, it allows for the demonstration of the crud and corrosion models on a core-scale model.

4.2.3   Results

Multiple simulations were performed with the Seabrook cycle 5 model to test and demonstrate the VERA CILC capability using the ROTHCON process and multiple corrosion model options. The results focus on those related to CILC, including the distribution of the maximum crud and corrosion thicknesses calculated by the simulations. Eight simulations were run to test the ROTHCON process with varying azimuthal and axial resolution against the basic Yao–Hochreiter–Leech (YHL) heat transfer model. Two different corrosion modeling options were also tested. A summary of the models and options used, along with the results for the maximum crud and corrosion thicknesses and the core crud mass, is shown in Table 8.

The YHL model is used as a baseline and is currently the default in VERA models because it does not require grid-design–specific CFD thermal hydraulic data. While the YHL model is not grid-design specific, it does allow VERA to capture a generic grid effect on the heat transfer and turbulent kinetic energy of the fluid immediately downstream from a grid. The naming convention for the coupling mesh resolution is consistent with previous sections in this report, with it being expressed as the number of sub-azimuthal by sub-axial surfaces.

As shown in Figures 20a–20d, the increase in coupling mesh resolution captures greater detail of the local conditions on the rod surface, leading to higher maximum crud and corrosion thickness and lower minimum crud and corrosion thicknesses. This result is confirmed in the quarter core case, as shown in Table 8. The "Corrosion Options" column in Table 8 shows the two sets of options used in the Seabrook cycle 5 simulations. The "Basic" option is the corrosion model that is common to CTF and Cicada, as described by Equations 1–3. The "Li + k_{ZrO_2}" corrosion option uses the corrosion model in CTF that includes the effect of lithium accelerated cladding corrosion factor described in Equations 5–6, along with the lower MATPRO cladding oxide thermal conductivity fit shown in Figure 13. Both of these additional options combine to significantly increase the total corrosion oxide thickness.

The increase in corrosion oxide is present in all cases when comparing simulations with the same heat transfer models but different corrosion options. Using the "Li + k_{ZrO_2}" increases the maximum corrosion oxide thickness from $16.84\,\mu m$ to $46.26\,\mu m$ for the 2×2 case. This is an increase of $175\,\%$. It should be noted that the YHL model provides good agreement with the ROTHCON models up to 4×4 resolution for the maximum crud and corrosion thicknesses. The different heat transfer models and corrosion models affect not only the maximum crud and corrosion thicknesses, but also the total crud mass present in the core. The core crud mass increases, similar to the maximum crud and corrosion thicknesses, as the coupling mesh resolution is increased. The YHL model differs significantly from the ROTHCON simulation results. This is due to the generic nature of the YHL heat transfer downstream from the grid. The reduction in core crud mass when using CFD data over YHL should be further investigated.

The maximum crud and corrosion thickness results have been visualized using VERAView and are shown in Figures 22–23. The figures show both a radial and an axial slice of the core at the maximum thickness location. The visualized results are from the end of cycle for the ROTHCON 4×4 case.
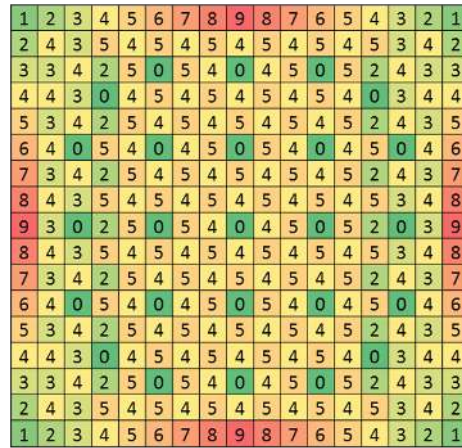
Figure 21. Graphical representation showing the pin indices taken from the WEC 5 × 5 CFD data to generate a functional map of pins with CFD data in a 17 × 17 fuel assembly configuration. These data are for demonstration of the quarter core simulations only and do not reflect the flow conditions inside the Seabrook Cycle 5 fuel assemblies.

Table 8. Summary of crud and corrosion results for varying heat transfer model and corrosion model options.

Heat transfer model option	Corrosion model options	Max crud thickness [μm]	Max corrosion thickness [μm]	Core crud mass [kg]
YHL	Basic	90.31	16.83	14.97
ROTHCON 1 x 1	Basic	90.31	16.76	9.91
ROTHCON 2 x 2	Basic	89.71	16.84	10.13
YHL	Li + k_{ZrO_2}	91.15	46.09	14.97
ROTHCON 1 x 1	Li + k_{ZrO_2}	89.71	45.21	9.91
ROTHCON 2 x 2	Li + k_{ZrO_2}	91.15	46.26	10.13
ROTHCON 4 x 4	Li + k_{ZrO_2}	91.85	46.86	10.27
ROTHCON 8 x 4	Li + k_{ZrO_2}	95.26	46.91	10.34

Figure 22. Distribution of the maximum crud thicknesses per rod per axial level for the quarter core simulation of Seabrook Cycle 5.

Figure 23. Distribution of the maximum corrosion thicknesses per rod per axial level for the quarter core simulation of Seabrook Cycle 5.

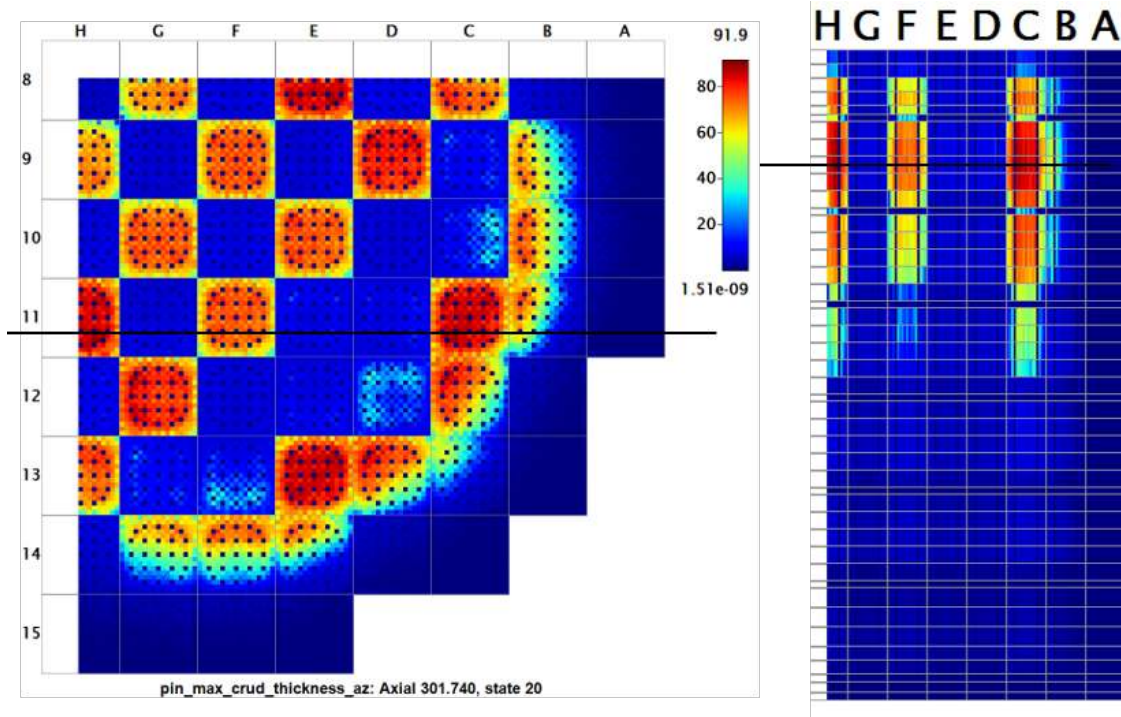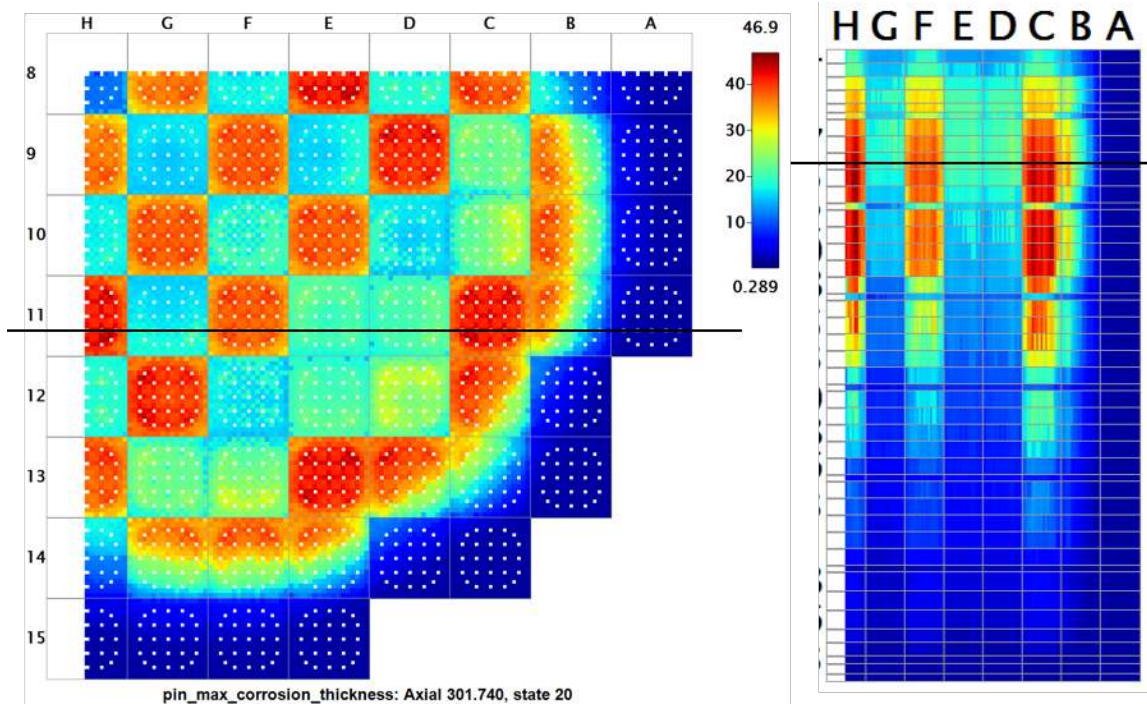The crud deposition shown in Figure 22 has a maximum thickness of 91.9 μm. The crud is mainly present in the fresh fuel assemblies, which is highlighted in the radial slice of the core. The axial slice shows a nominal crud distribution, with the majority of the crud being deposited in the upper spans of the core. This observation was also made during the fuel rod post-cycle examinations. The effects of the grid spacers are evident from the sharp decrease in crud buildup at those axial locations. This observation is also supported by post-cycle fuel rod examinations. Many fuel assemblies that have little-to-no crud buildup present due to low or no sub-cooled nucleate boiling on the surfaces of the rods in these lower power assemblies.

The corrosion distribution in the core, shown in Figure 23, is a core-wide phenomenon. This is because corrosion growth is temperature driven, while the crud buildup is strongly dependent on surface boiling. However, there is a strong positive correlation of corrosion thickness with crud thickness, because the thicker crud creates higher thermal resistance, thereby increasing the temperature of the cladding at those locations. Significant corrosion thicknesses can be seen below the mid-plane, while the crud does not deposit that low in the core. This is due to the increased cladding temperature in the middle of the core axially due to the higher power peaking at those locations.

A quantitative axial plot of the crud thickness and corrosion thickness for a single pin exhibiting this behavior is shown in Figure 24. The effects of the increased heat transfer due to the presence of the grids is evident as sharp decreases in both crud and corrosion thicknesses at these axial levels. The bottom 3 spans of the core have less than 10 μm of crud, while spans 5,6 and 7 have over 75 μm. The maximum crud thicknesses were calibrated using a sub-cooled nucleate boiling pre-factor term in the chemistry code MAMBA. The targeted maximum crud thickness was between 85 μm–95 μm because the crud scrape data showed a crud flake with a measured thickness of 82 μm from a fuel rod on the outside of the bundle. This calibration provided a crud thickness close to reality as part of the boundary condition for the corrosion models. While the maximum crud and corrosion thickness locations do not directly align, there is a strong positive correlation between increased crud thickness and increased corrosion oxide thickness. Overall, the maximum corrosion thickness is lower than expected for this cycle, with approximately correct crud thicknesses. Future work on the oxide corrosion modeling capability should be performed.

A plot of the crud and corrosion thickness buildup over time is shown in Figure 25. The x-axis corresponds to the statepoints shown in Table 7. The y-axis has units of micrometers and applies to both the crud and corrosion thicknesses. Note that the statepoints are not defined linearly with time. The first 100 EFPD are spread out over the first 12 statepoints, while the remaining 8 statepoints encompass 400 EFPD. Both the crud and the corrosion thicknesses start off growing slowly over the first 50–100 EFPD. Then they both transition to nearly a linear growth rate for the remainder of the cycle. Note that the corrosion growth rate transition is dependent on the oxide thickness. For these simulations, all initial corrosion oxide layer is assumed to be zero. The oxide growth rate transition occurs at approximately 2 μm. This suggests that the corrosion model could be sensitive to the initial thickness of the oxide layer on the fuel rod. Data on the initial oxide layer present on fresh fuel should be investigated and used to further inform the VERA corrosion models.

A pin census was performed for the lowest and highest resolution ROTHCON simulations using the "Li + k$_{ZrO_2}$" corrosion model option. The pin census was performed to investigate the effect of increasing the coupling mesh resolution on the number or fuel rods that have crud or corrosion thicknesses in excess of user-defined threshold limits. The threshold limits used in the pin census for the crud thickness were 85.2 μm and 90.5 μm, corresponding to the top 5 % of crud thicknesses in the core for the ROTHCON 1×1 and 8×4 cases, respectively. The threshold limits used in the pin census for the corrosion thickness were 42.9 μm and 44.6 μm, corresponding to the top 5 % of corrosion thicknesses in the core for the ROTHCON 1×1 and 8×4 cases, respectively. Table 9 shows that there is a large increase in the number of fuel rods that exceed the threshold criteria when the limit from the ROTHCON 1×1 case is used as an absolute threshold value for the ROTHCON 8×4 case. This supports the previous conclusions that the increased resolution of the coupling mesh leads to more fuel rods with greater maximum crud and corrosion thicknesses due to very localized thermal hydraulic conditions that are not captured with the more coarse coupling meshes. This result emphasizes the importance of resolving some of the local conditions with CFD informed data in order to perform effective CILC risk analysis for a core.
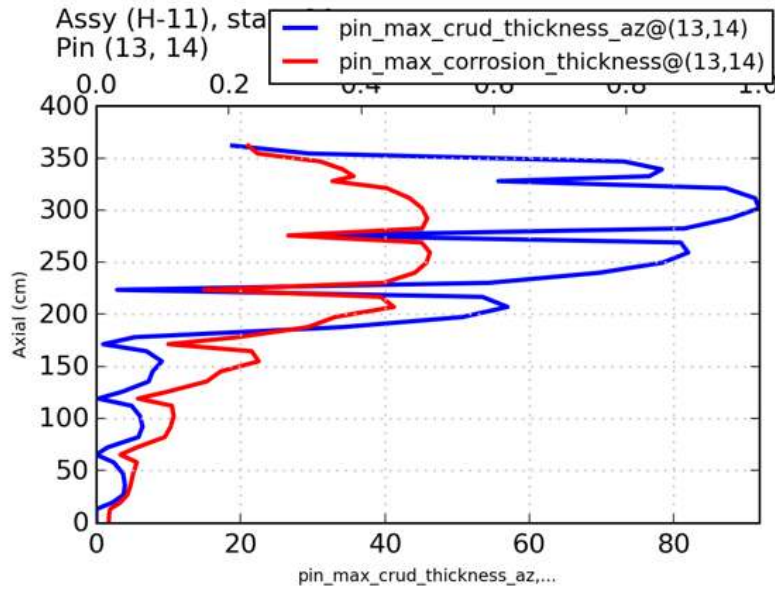
Figure 24. Axial plot of the maximum crud and maximum corrosion thicknesses for rod (13,14) in assembly C-11 in the Seabrook cycle 5 quarter core simulation.
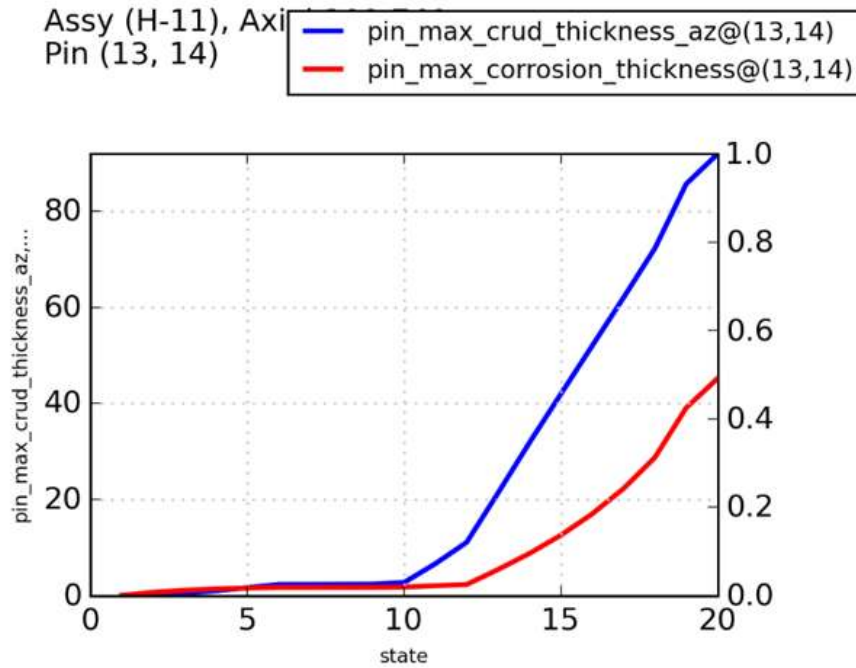

Figure 25. Plot of the maximum crud and maximum corrosion thicknesses for rod (13,14) in assembly C-11 in the Seabrook quarter core simulation over time for cycle 5.

Table 9. Summary of crud and corrosion pin census results. Results show that 33 rods have crud thicker than the 95$^{\text{th}}$ percentile of maximum crud thickness in the core when using ROTHCON 1×1. When running ROTHCON 8×4, the number of rods exceeding this same threshold jumps to 322. When using the 8×4 maximum crud thickness, 28 rods are in the 95$^{\text{th}}$ percentile. Similar results are observed for corrosion thickness, with roughly five times as many rods exceeding the threshold value from the 1×1 case.

Heat transfer model option	Pin census			
	Crud threshold		Corrosion threshold	
	$>85.2\,\mu\text{m}$	$>90.5\,\mu\text{m}$	$>42.9\,\mu\text{m}$	$>44.6\,\mu\text{m}$
ROTHCON 1×1	33	-	64	-
ROTHCON 8×4	322	28	318	102

CASL's visualization tool VERAView can be used to assist in CILC risk assessment by setting the data scale to 95 % of the maximum crud thickness to highlight the rods with crud thicknesses in the top 5 %. This was performed for assembly H-11 for the case with 4×4 coupling mesh resolution and the Li + k$_{ZrO_2}$ corrosion model options and is shown in Figure 26. Figure 26a shows the distribution of absolute crud thickness while Figure 26b shows the highlighted rods that have maximum crud thicknesses in the top 5 % for core. The highlighted rods can be investigated more closely to assess the risk of CILC failure. Additional capabilities are planned for implementation into VERAView to support CILC risk assessment through visualization and internal pin census reports on user-defined threshold limits and filters.

The runtimes required for each simulation were documented and are shown in Table 10. The increased resolution of the fuel rod surface chemistry comes at a cost of increased runtime. The runtime increases as the coupling mesh is refined, regardless of what corrosion options are used. This is expected since the number of surface heat transfer and chemistry solves scales with the increased coupling mesh resolution. Although the coupling mesh refinement is applied to every fuel rod surface element in the core, the total runtimes for the higher resolution simulations do not scale directly one to one. For example, increasing the ROTHCON resolution from 1×1 to 8×4 is a resolution increase of 32. However, the runtime only increases by a factor of 5.7. As shown in Figure 11, there are diminishing returns in increased accuracy after a certain amount of resolution refinement. The larger runtimes with higher resolution must be balanced against the gain in accuracy of the surface thermal hydraulic conditions to provide optimal solution accuracy with a reasonable runtime. Investigation into performance improvements to decrease runtimes while maintaining accuracy in the regions of interest for crud and corrosion should be performed. Flexibility in applying the ROTHCON maps to specific locations in the core (such as individual pins or above a user-defined axial level) could decrease the runtimes by not solving high resolution surface effects in areas that are not of interest to CILC.

Overall, a successful preliminary demonstration was performed with the application of the ROTHCON maps in varying degrees of resolution with multiple corrosion model options to a VERA model of Seabrook cycle 5. This capability provides the foundation for a CILC risk assessment tool that can be validated with past reactor cycles and applied in future core design processes for operating nuclear power plants.
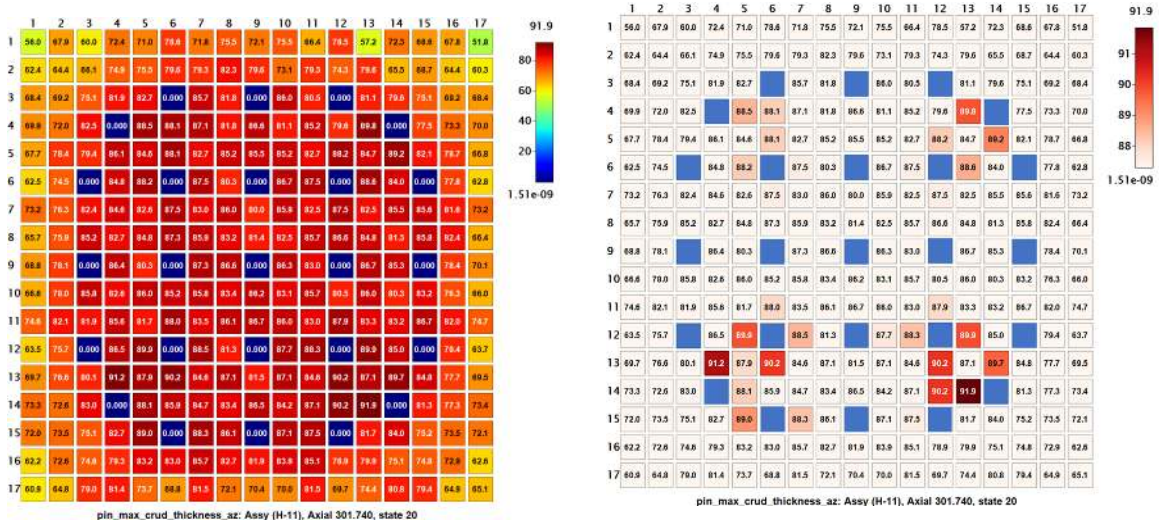
(a) Assembly H-11 maximum crud thickness distribution.

(b) Rods in assembly H-11 that have been filtered and highlighted by VERAView with crud thickness in top 5 percent.

Figure 26. Use of VERAView to filter and highlight pins in assembly H-11 with maximum crud thickness in the top 5 percent. The rod highlighted in (b) are potential rods of concern for CILC. Guide tubes are shown in blue.

Table 10. Simulation run times for varying heat transfer model and corrosion options.

Heat transfer model option	Corrosion options	Runtime [m:s]
YHL	Basic	73:27
ROTHCON 1×1	Basic	70:48
ROTHCON 2×2	Basic	100:26
YHL	Li + k_{ZrO_2}	70:41
ROTHCON 1×1	Li + k_{ZrO_2}	69:00
ROTHCON 2×2	Li + k_{ZrO_2}	99:51
ROTHCON 4×4	Li + k_{ZrO_2}	220:00
ROTHCON 8×4	Li + k_{ZrO_2}	400:08

5 CONCLUSION

This milestone led to the successful creation of a preliminary CILC risk assessment capability in VERA-CS. This was completed by leveraging and further developing the existing CASL codes Cicada and MAMBA. Additionally, a clad oxidation model was implemented into the T/H subchannel code, CTF. The ROTHCON process for capturing higher fidelity rod surface heat transfer and turbulence behavior has been further developed so that it can be enabled by the VERA-CS user.

Several assessments have been performed to demonstrate the proper functioning of the tools that make up the VERA-CS CILC capability. Mesh refinement studies were performed on the ROTHCON process to demonstrate that the coupling mesh multiplier map properly converges to the input data and that rod surface temperature predictions properly converge to the expected STAR-CCM+ results used to generate the ROTHCON maps. The effect of using a 1D versus 3D modeling approach in Cicada was checked, and it was observed that less corrosion growth is predicted using the 3D approach. It was found that using 100 rings in the oxide region of the 3D modeling approach is sufficient for obtaining a converged solution, and this level of refinement has very little impact on the simulation walltime when compared to the 1D solution.

The effect of crud lithium concentration and oxide thermal conductivity on oxide growth was checked. It was found that lithium concentration has a significant impact on oxide growth and should be included in the model. Future work will involve adding this effect to the Cicada oxide model.

A mesh refinement study was performed to test the effect of the ROTHCON coupling mesh refinement on maximum predicted crud and corrosion growth in a rod bundle. It was shown that the coupling mesh can have a significant impact on whether or not a rod experiences crud/corrosion growth, which rod experiences the maximum crud/corrosion growth, and the magnitude of the maximum crud/corrosion thickness. It was generally observed that as the mesh is refined, low heat transfer areas are better resolved, which leads to overall larger maximums in crud and corrosion thickness when compared to lower resolution meshes.

Finally, a demonstration of the VERA-CS CILC capability was made for its intended use-case of running a quarter core, pin-resolved cycle depletion simulation. The Seabrook Cycle 5 model was used to perform the demonstration. Because CFD data are not yet available for the Seabrook spacer grid design, a mock dataset was constructed from the 5×5 bundle data. While it is not possible to do a thorough analysis of the data due to the lack of proper data for the ROTHCON model, some conclusions can be drawn. It was found that maximum corrosion thicknesses were generally less than anticipated, which points to a need for future work in developing the corrosion modeling capability. Results have shown that the ROTHCON coupling mesh refinement has a small impact on total core crud mass, causing it to increase by about 5% when going from no refinement to high refinement. However, when compared to the existing grid heat transfer enhancement model in CTF (YHL), there is about a 50% reduction in total core crud mass, which warrants further investigation. The core maximum crud thickness increases by 6%, and the core maximum corrosion thickness increases by 4% when going from no refinement to high refinement. While the maximum thickness increases only a slight amount with application of the ROTHCON process, it was found that the number of pins exceeding a set upper threshold thickness increased by a considerable amount, which is the behavior that was observed for the smaller 5×5 assessment.

Future work for the CILC capability will include implementing aforementioned modeling improvements to Cicada, including restart features and the corrosion lithium effect. There will also be a need for performance improvements. It was discovered during the full-core demonstration that going to 8×8 coupling mesh refinement when using ROTHCON led to an out-of-memory error on the CADES cluster, prompting a reduction in the refinement level to 8×4. Reducing the amount of data retained by the ROTHCON feature during runtime should address this issue. The quarter core demonstration also revealed that the total simulation walltime increases by roughly a factor of 5–6 when going from 1×1 to 8×4 coupling mesh refinement. This will need to be reduced if the ROTHCON process becomes part of standard CILC analyses.

Validation of the capability will also be needed, which is already planned to take place in upcoming milestones to assess the accuracy of MAMBA crud growth and its predictions. A criterion must be developed to identify pins at risk for CILC, as well. This criterion must be implemented into the VERA-CS simulation workflow to make it easy for the user to perform the CILC risk assessment. VERA-CS CILC risk assessments using the developed capability and risk criterion must be performed with comparisons made to plant data. Validation assessments should include plants with and without CILC risk, as well as plants that have experienced CILC failures, to properly assess the accuracy of and further refine the developed capability.

ACKNOWLEDGMENTS

References

[1] Arthur T. Motta, Adrien Couet, and Robert J. Comstock. "Corrosion of Zirconium Alloys Used for Nuclear Fuel Cladding". In *Annual Review of Materials Research* 45.1 (2015), pp. 311–343.

[2] T.J. Abram. *Modeling the waterside corrosion of PWR fuel rods*. Tech. rep. IAEA-TECDOC–957. International Atomic Energy Agency (IAEA), 1997.

[3] B. Collins et al. *Development of a Comprehensive CRUD-Induced Power Shift (CIPS) Capability within VERA*. Tech. rep. CASL-X-2017-1406-000. Consortium for Advanced Simulation of Light Water Reactors, 2017.

[4] B. Collins et al. "Simulation of Crud Induced Power Shift using the VERA Core Simulator and MAMBA". In *PHYSOR 2016*. 2016.

[5] S. Slattery and W. Gurecky. *Support for CILC L1 Milestone Using STAR-CMM+*. Tech. rep. L3:PHI.CMD.P12.02. Consortium for Advanced Simulation of Light Water Reactors, 2016.

[6] A. Manera et al. *Qualification of CFD-based PWR CILC capabilities for the identification of high-risk fuel rods*. Tech. rep. CASL-U-2016-1195-000. Consortium for Advanced Simulation of Light Water Reactors, 2016.

[7] S. Slattery, R. Salko, and K. Clarno. *The Effect of Subchannel vs. CFD Discretizations on CRUD Growth using MAMBA1D*. Tech. rep. Consortium for Advanced Simulation of Light Water Reactors, 2015.

[8] R. Salko et al. "Implementation of a Grid Heat Transfer Hi2lo Reconstruction Capability into the Thermal Hydraulics Subchannel Code CTF". In *ANS Best Estimate Plus Uncertainty International Conference (BEPU 2018)*. 2018.

[9] S. Slattery, W. Gurecky, and Ni. Adamowicz. *L4:PHI.CMD.P14.01*. Tech. rep. CASL-U-2017-1400-000. Consortium for Advanced Simulation of Light Water Reactors, 2017.

[10] R. Salko et al. *Implementation of a Grid Heat Transfer and Turbulent Kinetic Energy Hi2Lo Remapping Capability into CTF in Support of the CIPS Challenge Problem*. Tech. rep. CASL-U-2017-1322-000. Consortium for Advanced Simulation of Light Water Reactors, 2017.

[11] R. Salko et al. *Summary of CTF Accuracy and Fidelity Improvements in FY17*. Tech. rep. CASL-U-2017-1428-000. Consortium for Advanced Simulation of Light Water Reactors, 2017.

[12] *Waterside corrosion of zirconium alloys in nuclear power plants*. Tech. rep. IAEA-TECDOC-996. International Atomic Energy Agency, 1998.

[13] *EPRI PWR Fuel Cladding Corrosion (PFCC) Model Volume 2: Corrosion Theory and Rate Equation Development*. Tech. rep. TR-105387-V2. EPRI Palo Alto, CA, 1996.

[14] W.G. Luscher, K.J. Geelhood, and I.E.A Porter. *Material Property Correlations: Comparisons between FRAPCON-4.0, FRAPTRAN-2.0, and MATPRO*. Tech. rep. PNNL-19417 Rev. 2. Pacific Northwest National Laboratory, 2015.

[15] D. Pointer. *Reference Computational Meshing Strategy for Computational Fluid Dynamics Simulation of Departure from Nucleate Boiling*. Tech. rep. CASL-U-2017-1390-000. Consortium for Advanced Simulation of Light Water Reactors, 2017.

[16] *Description of Mixing Vane Grid CHF test for CASL DNB Challenge Problem*. Tech. rep. PFT-16-3, Rev.1. 2016.